MICHIGAN STATE UNIVERSITY

CYCLOTRON LABORATORY

SHELL MODEL CALCULATIONS FOR EXOTIC NUCLEI

B.A. BROWN, E.K. WARBURTON, and B.H. WILDENTHAL

FEBRUARY 1990

MSUCL-715

MSUCL-715
February, 1990

Shell Model Calculations for Exotic Nuclei [1]

B. A. Brown

Cyclotron Laboratory and Department of Physics and Astronomy
Michigan State University, East Lansing, Michigan 48824

E. K. Warburton

Brookhaven National Laboratory, Upton, New York 11973

B. H. Wildenthal

Department of Physics and Astronomy
University of New Mexico, Albuquerque, New Mexico, 87131

1. INTRODUCTION

In this paper we review the progress of the shell-model approach to understanding the properties of light exotic nuclei (A<40). By "shell-model" we mean the consistent and large-scale application of the classic methods discussed, for example, in the book of de-Shalit and Talmi (Ref 1). Modern calculations incorporate as many of the important configurations as possible and make use of realistic effective interactions for the valence nucleons (Ref 2). Properties such as the nuclear densities depend on the mean-field potential, which is usually treated separately from the valence interaction. We will discuss results for radii which are baaed on a standard Hartree-Fock approach with Skyrme-type interactions (Ref 3).

With the present generation of shell-model codes run on VAX computers, treatment of cases with J-scheme dimensions of up to about 7,000 is routine (Ref 4). At this level we are able to consider the full basis for both protons and neutrons in the Op or 1s0d major shells, as well as for protons in the Op shell combined with neutrons in the 1s0d shell. For many cases in which protons in the 1s0d shell are combined with neutrons in the 1p0f shell, the dimensions are already over 7000. However, many interesting sd-pf cases are possible, and we have considered a few cases in the sd-pf model space with dimensions up to about 12,000 (Ref 5).

---

[1] Invited talk presented by Alex Brown at the American Chemical Society Symposium on Exotic Nuclear Spectroscopy, 11-16 Sept., 1989, Miami, Florida, and at the Workshop on Nuclear Structure of Light Nuclei Far from Stability, 27-29 Nov., 1989, Obernai, France.

Table 1: Table of model spaces and interactions

Model space	Interaction	Type	Code	
0p (p)	Cohen-Kurath	TBME	CK	Ref 6
	Millener	POT	M	Ref 7
1s0d (sd)	Wildenthal	TBME+G	W	Ref 8
	Brown et al.	POT	SDPOTA	Ref 9
1p0f (pf)	McGrory	TBME+G	MG	Ref 10
p-sd	Poppelier et al.	TI	PG	Ref 11
	Millener-Kurath	POT	MK	Ref 12
sd-pf	Warburton et al.	POT	WBMB	Ref 13

In Table I we summarize the model spaces and interactions used in the discussions. We give the interactions used within the major shells (p, sd and pf) and the cross-shell interaction for the combined shells (p-sd and sd-pf). The total interaction in the combined shells may be unified, as in the case of the PG interaction, or it may be composed of three parts representing the components within the two major shell plus the cross terms. The ones of this type discussed here are M-W-MK for the region $2 \leq Z \leq 8$ and $8 \leq N \leq 20$ and W-MG-WBMB for $8 \leq Z \leq 20$ and $20 \leq N \leq 40$.

All interactions have been adjusted by a least-squares fit to some selection of binding energy and excitation energy data (the fit-data set). This was accomplished by varying the individual two-body matrix elements (TBME), by varying the well determined linear combinations of two-body matrix elements and keeping the rest fixed at some G matrix values (TBME+G), by varying parameters of some potential (POT), or by varying the Talmi integrals (TI). We note that all of these effective interactions are very close to that expected from microscopic G-matrix calculations based on the nucleon-nucleon interaction, but that the small differences from the G matrix are very important for detailed spectroscopy (Ref 2 and Ref 4).

Within the above framework we are able in principle to discuss all observed properties of the exotic nuclei. Many of these properties will now be discussed, roughly in order of increasing complexity. First, the binding energy systematics of neutron rich nuclei are discussed in the framework of $0\hbar\omega$ shell-model configurations (Sec. 2). "$0\hbar\omega$" means that the nucleons are

assumed to fill the lowest available major-shell configurations. The deviation between experiment and theory in this context for nuclei around ^{32}Mg will then be addressed in terms of cross-shell ($n\hbar\omega$) excitations (Sec. 3). Next we discuss the β decay properties, starting with half-life comparisons and going into some details of the Gamow-Teller strength functions and the subsequent delayed particle emission (Sec. 4). Finally, we address the question of the large radii and large Coulomb break-up cross sections found for the neutron rich Li and Be isotopes (Sec. 5). Summaries will be included in each section.

2. BINDING ENERGIES

The first property usually measured for the most exotic nuclei is whether or not they are bound to nucleon decay. When a nucleus is bound to nucleon decay it can only decay by the weak interaction and will have a half-life on the order of milliseconds or greater. This will be referred to as a "stable" nucleus in the discussion below. A nucleus which does decay by nucleon emission will be referred to as "unstable." If a nucleus is stable its mass excess can be measured. Even for unstable nuclei, the mass excess of the ground and excited states can be measured by transfer reactions if the appropriate target is available. The only important nucleon-decay channel for the ground states of unstable neutron-rich nuclei is neutron emission. The Q values for these decays can be inferred easily from the binding energy plots shown below.

2.1 p and p-sd model spaces

The He isotopes were recently studied by the MSU group where ^{10}He was not observed and thus is most probably unstable (Ref 14). In Fig. 1 We show the experimental binding energies for the ground and excited states of the He isotopes compared to a recent p-shell calculation. In this calculation three parameters of a potential model for the interaction and the two single-particle removal energies (SPRE) were fitted to the eight known data including the binding energy of ^{9}He obtained from a pion double-charge-exchange reaction (Ref 15). The fit is good for the known states and in agreement with the experimental prediction that ^{10}He is unstable. In the calculation, ^{10}He is clearly unbound to two-neutron emission and may or may not be bound to one-neutron emission.

In the extreme j-j coupling limit, the He binding energies can be interpreted in the shell model as follows. The $p_{3/2}$ SPRE, as determined by the

^{5}He(ground state)-^{4}He energy difference, and the $p_{1/2}$ SPRE, as determined from the ^{5}He(excited state)-^{4}He energy difference, are both negative (unbound). The ^{6}He-^{4}He binding energy difference is then two times the $p_{3/2}$ SPRE (which by itself would make ^{6}He unbound) plus the pairing energy in the $(p_{3/2})^2$ configuration. This latter term is positive (attractive) and large enough to make ^{6}He bound. If ^{8}He has a pure $(p_{3/2})^4$ configuration, the effective $p_{3/2}$ SPRE is given by the ^{8}He-^{7}He energy difference. This is seen to be positive as a result of the addition of the residual interaction within the $p_{3/2}$ shell. Similarly, the effective $p_{1/2}$ SPRE given by the ^{9}He-^{8}He energy difference is negative but less so than it was in ^{5}He-^{4}He. Finally, we see that ^{10}He is unstable because the positive pairing energy for the $(p_{1/2})^2$ configuration is weaker than it was for ^{6}He and not strong enough to make up for the two times the negative $p_{1/2}$ SPRE contribution. The calculations shown in Fig. 1 are more complicated than this extreme j-j coupling picture since they take all p-shell configurations into account. However, the dominant components of the wavefunctions are those assumed above, and thus the qualitative features of the discussion still hold.

The neutron rich Li, Be, B, C and N nuclei have been experimentally studied all the way to the neutron drip line (Ref 16, Ref 17 and Ref 18). Poppelier et al. (Ref 11) have made binding energy comparisons between the p-sd PG calculations and experiment. Vieira (Ref 19) has made binding energy comparisons between their p-sd M-W-MK calculations and experiment. In both cases there are differences of up to 2 MeV between experiment and theory, and because of this there are several cases where the predicted stability property is in disagreement with experiment. The calculations could probably be improved by use of a better effective interaction, but the limit within the model is probably around the 0.5 MeV rms deviation obtained for the well-known p-shell nuclei (Ref 6).

2.2 sd and sd-pf model spaces

There has been excitement recently about the apparent instability of ^{26}O (Ref 16). We show in Fig. 2 binding energy curves for the O isotopes. The experimental data are compared with three predictions: the global predictions of Moeller and Nix (Ref 20), the W-sd calculation up to N=20 plus the W-MG-WBMB-sd-pf calculation beyond N=20, and the SDPOTA-sd calculation. The shell-model predictions are clearly better than the global-model

predictions in this case. The average deviation between the shell-model predictions and experiment is consistent with the average 180 keV rms deviation found for 447 ground and excited states over the entire sd shell (Ref 2 and Ref 8). The global model of Moeller and Nix as well as most other global models (Ref 21) predict that ^{26}O is stable in contradiction to experiment. However, this is not too surprising, given the rather poor agreement for the other O isotopes. It is more surprising that the W-sd calculations also predicts that ^{26}O is stable by about 1 MeV. However, the SDPOTA-sd calculation predicts ^{26}O to be unstable, but only by 20 keV! This difference is an indication of the rather large model dependence which can exist in the shell-model extrapolations to exotic nuclei. With both W and SDPOTA ^{27}O and ^{28}O are predicted to be unstable. We now discuss some aspects of the model dependence.

The trend of the O binding energies can be understood in the extreme j-j coupling limit in much the same way as was discussed for the He isotopes. We show in Fig. 3 the effective neutron single-particle energy (ESPE) as a function of neutron number in this j-j coupling limit. (By convention, ESPE = -SPRE, where SPRE is the single-particle removal energy used in the discussion for the He isotopes.) The neutron ESPE are seen to be rather constant as a function of neutron number. This leads to a simple qualitative interpretation for the binding energy curve shown in Fig. 1. Between N=8 and 14 the neutrons fill the $d_{5/2}$ orbit which is bound in ^{16}O by about 4 MeV. This, together with the attactive pairing energy, provides the sharp increase in binding energy observed between N=8 and 14. Between N=14 and 16 the neutrons fill the $s_{1/2}$ orbit which is less bound than the $d_{5/2}$. Thus one starts to see less increase in the binding energy at this point. Between N=16 and 20 the neutrons fill the $d_{3/2}$ orbit which has close to zero energy, and the binding energy curve becomes flat in this region. This flatness, of course, makes it difficult to predict exactly which nuclei will be stable, which is what makes this region so interesting from the stability point of view. Beyond N=20 the neutrons must start to go into the pf shell orbits which are unbound. Hence the binding energy curve decreases beyond this point. This marks the end of where the O isotopes can be studied and also the end of where they need to be understood for astrophysical purposes.

At the next level of detail we should take into account the small shifts in the neutron ESPE shown in Fig. 3. These are again due to the interactions within the shells. For example the shift in the $s_{1/2}$ ESPE between ^{16}0 and

^{22}O is due the monopole average over two-body matrix elements:

$$\Sigma_J\ (2J+1) <d_{5/2},s_{1/2},J|V|d_{5/2},s_{1/2},J> / \Sigma_J\ (2J+1)$$

It is important to note that these two-body matrix elements can in principle be obtained from information on excited states in ^{18}O and ^{19}O etc. Data on excitation energies relevant to these $d_{5/2}$-$s_{1/2}$ two-body matrix elements were included in the 447 fit-data set used to obtained the W and SDPOTA interactions. Hence, the good agreement for the ^{23}O and ^{24}O mass predictions may not be surprising even though data on these two nuclei were not included in the fit-data set. In contrast, beyond ^{24}O, the ESPE depend on the $d_{5/2}$-$d_{3/2}$ two-body matrix elements. Data on excitation energies relevant to these do not exist because they are more highly excited configurations and lie in a large level density of intruder states. Hence beyond ^{24}O, the predictions rely more on assumptions in the calculation which cannot be tested from previously known data. For the W interaction this is the Kuo-Brown G matrix used for the poorly determined linear combinations, and for the SDPOTA interaction this is the particular form of the potential model assumed (a modified surface one-boson exchange potential).

The actual sd-shell calculations shown in Fig. 2 go beyond j-j coupling and include all possible sd-shell configurations. But again, the dominant configurations are those assumed above. These calculations, it should be remembered, are based on zeroth-order perturbation theory together with an assumed constancy of the bare SPE and an assumed simple $(A/18)^{0.3}$ mass dependence of the two-body matrix elements (Ref 2 and Ref 8). Presumably nature is more complicated than this. But, given the continued success of the shell-model in correlating essentially all observed data, these complications must get folded into the effective nature of the interactions in a way that may never be fully quantitatively understood.

In contrast to the relative constancy of the neutron ESPE as a function of neutron number, they quickly decrease as a function of proton number, as shown in Fig. 4 for N=20 and Z=8 to 20. By the time one reaches ^{40}Ca all of the sd-shell orbits as well as the pf-shell orbits are bound. At N=20 the ESPE of the neutron orbits as a function of N should again be relatively constant, and applying the same qualitative argument as above, we can see that all Ca isotopes out to ^{60}Ca should be stable. The stability in the region between ^{60}Ca and ^{70}Ca depends on exactly what the value of the ESPE for

the $g_{9/2}$ orbit is at this point.

Binding-energy comparisons have been made for Z=9-20 similar to the ones shown in Fig. 2 for O. We show the differences between experiment and the theoretical predictions in Fig. 5. The predictions are based on W-sd for N$\leq$20 and W-MG-WBMB-sd-pf for N>20. New data on the F and Ne isotopes have been included (Ref 22).

We first discuss the stability properties which are not shown in Fig. 5. ^{28}F is predicted to be unstable and ^{29}F is predicted to be stable by both W and SDPOTA in agreement with experiment (Ref 16). W-MG-WBMB predicts all F nuclei to be unstable beyond this point. ^{29}Ne is predicted to be unstable by 129 keV with the W interaction and by 4 keV with the SDPOTA interaction. Hence the disagreement with experiment (Ref 16) is not too surprising. ^{30}Ne and ^{32}Ne are predicted to be stable and ^{31}Ne unstable in agreement with experiment. Beyond these only ^{34}Ne is predicted to be stable. All remaining nuclei in the sd-shell (N$\leq$20) for Z>10 are predicted to be stable, in agreement with experiment. And for N>20 and Z>10 the W-MG-WBMB calculations have not yet been carried out far enough in neutron number to predict where the drip line is.

The differences shown in Fig. 5 show excellent agreement between experiment and theory for most cases. Again we emphasize that the shell-model is a successful model for excitation energies as well as ground state masses. To emphasize this point we show in Fig. 6, the predicted and experimental excitation energies for ^{27}Al (Ref 23). The quality of agreement shown for ^{27}Al holds for levels up to about 8 MeV in all sd-shell nuclei near the valley of stability.

There are some exceptional deviations in Fig. 5. For N=18 and 9$\leq$Z$\leq$13 there is a pronounced glitch which may be due to a similar kind of model-dependence left in the W interaction as discussed above for ^{26}O. The more dramatic deviations in the most neutron rich Na and Mg isotopes, which have been known for many years (Ref 24), point to the intruder state problem which is discussed in the next section.

The next major step in the sd-shell calculations will be to incorporate all of the new data which has appeared since the original fit-data set was put together about ten years ago.

3. CROSS-SHELL EXCITATIONS AROUND ^{32}MG

The anomalies in the binding energies, excitation energies, half-lives and radii of the most neutron rich Na and Mg isotopes relative to the type of $0\hbar\omega$ calculations described above have been known for a long time (Ref 24). The situation has been referred to as the "collapse of the conventional shell model" (Ref 25). Several studies over the past ten years have indicated that the problem is due to low-lying intruder states from the pf shell (Ref 26, Ref 27 and Ref 28). We report here on a new set of systematic calculations with the W-MG-WBMB interaction for these intruder states (Ref 5). These new calculations incorporate all of the sd and pf orbits and represent the most ambitious calculations to date. An advantage (and disadvantage) of our calculations is that there are no adjustable parameters. The W-sd and MG-pf parts of the interactions were already well established. The WBMB cross-shell interaction (Ref 13) was obtained from a fit of the Millener-Kurath potential model (Ref 12) parameters and some fine tuning of some individual two-body matrix to reproduce the excitation energies of 1p-1h states in ^{40}Ca and ^{40}K.

An important aspect of our calculations is that we do not allow for explicit mixing between $0\hbar\omega$, $2\hbar\omega$, $4\hbar\omega$, etc. configurations or between $1\hbar\omega$, $3\hbar\omega$ etc. configurations. The rationale for this restriction is related to the "excitation-order" problem discussed in Ref 2 and is discussed more in the present context in Ref 5. The standard shell-model interactions we are familiar with, such as the W-sd interaction, are designed to reproduce binding energies without such explicit mixing and must already incorporate this mixing implicitly. Our experience with the well-known $n\hbar\omega$ intruder states near ^{16}O and ^{40}Ca indicates that these different excitations tend to "coexist" rather than to strongly mix with each other. Our point of view is that we do not at present know how to deal with explicit mixing and that hopefully "coexistence" will continue to hold.

This is one of the major differences between our calculations and those of Poves and Retamosa where explicit mixing between major shells is allowed. Poves and Retamosa mix an extremely deformed $2\hbar\omega$ ground state band (e.g. with the 2^+ energy around 200 keV) with the normal $0\hbar\omega$ states to get resulting spectra which are moderately deformed (e.g. with the 2^+ energy around 800 keV). Our calculation, with no mixing, and the Poves-Retamosa

calculation, with large mixing, give qualitatively the same spectra in cases where the experimental data were known before the calculation. We will point out at the end of this section several places where important differences between the calculations are expected which could be tested experimentally.

3.1 Weak-coupling aspects

In our study of the ^{32}Mg region, we first calculated all of the $0\hbar\omega$ and $1\hbar\omega$ spectra which had dimensions less than about 12,000. Comparison to experiment for the $Z \geq 14$ region was good (Ref 29 and Ref 30). However, as discussed in the last section, the calculated $0\hbar\omega$ binding energies in the region of ^{32}Mg are markedly smaller than experiment. We next looked at $n\hbar\omega$ excitations for N=20 and Z<14. Full space $1\hbar\omega$ and $2\hbar\omega$ sd-pf calculations are possible for ^{28}O, ^{29}F and ^{30}Ne. From these studies we determined that the proton excitations from sd to pf could safely be ignored. The important state was found to correspond to a $2\hbar\omega$ neutron excitation. This state had an excitation energy relative to the lowest $0\hbar\omega$ state in these three nuclei of 2.96 MeV, 1.34 MeV, and -0.79 MeV, respectively. The full-space calculations for most of the nuclei of interest around ^{32}Mg have dimensions which are too large to handle. We investigated several truncations which have promise for future calculations. However, the most interesting and useful result found in these investigations is that a weak-coupling model can be used to relate the excitation energy of the $n\hbar\omega$ configurations to the calculated $0\hbar\omega$ binding energies in nuclei with neighboring neutron numbers.

Many examples, of the weak-coupling model have been discussed for nuclei around ^{16}O and ^{40}Ca where the residual interaction between particles and holes has an isospin-dependence (Ref 31). In our case the form of the particle-hole interaction is much simpler since only neutrons are presumed to be excited. The motivation for the weak-coupling formula is as follows. Consider, as an example, the N=19 nucleus ^{31}Mg which has a $0\hbar\omega$ configuration of one neutron hole (1h) in the sd shell relative to the N=20 neutron closed shell. The $n\hbar\omega$ configuration then has the form $(\nu pf)^n$-$(\nu sd)^{-(n+1)}$. In analogy with the expression for 1-particle 1-hole states in closed shell nuclei, the energy of this $n\hbar\omega$ configuration relative to the N=20 closed shell is $E(19,n\hbar\omega) - E(20) = \epsilon(\text{n-particles}) - \epsilon[(n+1)\text{-holes}] - n(n+1)C$, where E(N) is the interaction energy of the $0\hbar\omega$ configurations (the negative of the binding energy) for the neutron number N (at a fixed Z), and where the last term

takes into account the average particle-hole interaction C between neutrons. The particle energy is given by ϵ(n-particles) = E(20+n) - E(20) and the hole energy is given by ϵ[(n+1)-holes] = E(20) - E(19-n). By combining these results we obtain $Ex^{wc}(19,n\hbar\omega)$ = E(19,n$\hbar\omega$) - E(19) = E(19-n) + E(20+n) - E(20) - E(19) - n(n+1)C. For N$\leq$20 this generalizes to

$$Ex^{wc}(N,n\hbar\omega) = E(N\text{-}n) + E(20+n) - E(N) + E(20) - n(20\text{-}N+n)C,$$

and for N>20

$$Ex^{wc}(N,n\hbar\omega) = E(N+n) + E(20\text{-}n) - E(N) + E(20) - n(N\text{-}20+n)C.$$

The weak-coupling model should be a valid approximation if the dominant interactions are taken into account by the E(N) and the residual interaction C is weak. This appears to be true in our case. Empirically we obtain C = 143 keV for Z=8 and C = 240 + 10(Z-9) keV otherwise. There is the additional assumption that the energies and structure of the multi-particle and multi-hole configurations do not change when they are coupled together.

The excitation energies for the $2\hbar\omega$ and $1\hbar\omega$ configurations based on the full space and weak-coupling models are compared in Fig. 7 and Fig. 8, respectively. In addition, in these figures we give the excitation energies in the weak-coupling model where the full basis calculation is not possible and in Fig. 8 we also give the $3\hbar\omega$ excitation in the weak-coupling model. Examination of Figs. 7 and 8 shows that the region of nuclei shown in Fig. 9 do not have $0\hbar\omega$ ground states, and we will refer to this as the "island of inversion."

3.2 Mechanisms for lowering the $n\hbar\omega$ excitations

We now discuss the mechanisms by which the $n\hbar\omega$ excitations are lowered in energy to create the island of inversion. The first aspect is the single-particle energy gap between the sd and pf shell. The neutron effective single-particle energies (ESPE) calculated with our interaction are given in Fig. 4. For ^{28}O (Z=8) and ^{40}Ca (Z=20) the results are exact and given by E(N=21) - E(N=20) for the pf particle states and by E(N=20) - E(N=19) for the sd hole state. For ^{34}Si (Z=14) and ^{36}S (Z=16) the results shown in Fig. 4 are approximate and obtained under the assumption that the protons have a subshell closure of $(d_{5/2})^6$ and $(d_{5/2})^6(s_{1/2})^2$, respectively. Our full calculations for ^{34}Si and ^{36}S include all possible sd-shell proton configurations.

The gap between sd and pf shells shows a moderate decrease from E_{gap} = 7239 keV in ^{40}Ca to 5115 KeV in ^{28}O. This is in contrast to the results of Storm et al. (Ref 28) which predict the gap actually becomes negative for ^{28}O. We see from Fig. 5 that our $0\hbar\omega$ mass predictions (and hence our ESPE) are in good agreement with experimental N=19, 20 and 21 binding energies from Z=20 to Z=13. Thus, we have some confidence in the correctness of our extrapolation from Z=12 to Z=8. We conclude that the decrease in the sd-pf gap contributes to, but is not the primary cause of, the inversion.

For proton excitations the gap between $d_{5/2}$ and $f_{7/2}$ is very large for ^{28}O (14.7 MeV), and the sd-pf excitations for protons can be ignored. Of course, the sd-pf gap is the same for protons and neutrons in ^{16}O and ^{40}Ca and both excitations must therefore be considered in these regions. However, we find that the the low-lying $2\hbar\omega$ states in ^{38}Ar are already dominated by the neutron excitations.

The excitation energies of the $1\hbar\omega$ neutron 1p-1h states in the N=20 isotones (see Fig. 8) are close to the gap energy E_{gap} in ^{28}O, ^{34}Si and ^{35}P. The lowering of the $1\hbar\omega$ excitation to 2404 keV in ^{31}Na and its increase back up to 4747 keV in ^{34}Si is an aspect of the correlation energy (but on a smaller scale) which will now be discussed in more detail for the $2\hbar\omega$ excitations in N=20 and the $1\hbar\omega$ excitations in N=19 and 21.

First we consider the $2\hbar\omega$ excitations for N=20. It can be seen from Fig. 7 that the excitation energy of the $2\hbar\omega$ neutron excitations is always much lower than two times the ESPE gap. Both the neutron-neutron interaction energy E_{nn} and the proton-neutron interaction energy E_{pn} contribute to this effect. Since the monopole interaction is taken into account by the changes in the ESPE, E_{nn} is primarily due to the residual "pairing" interaction. E_{nn} can be estimated from the calculated excitation energy of the 2p-2h state in ^{28}O; E_{nn} = Ex - 2x(E_{gap}) = 3038-2x(5115) keV = -7192 keV (with the weak-coupling estimate for Ex). Since E_{nn} depends only on the neutron configurations, we expect E_{nn} to be approximately independent of Z. Thus, the proton-neutron contribution E_{pn} as a function of Z can be estimated from E_{pn}(Z) = Ex(Z) - 2x(E_{gap}) - E_{nn} with E_{gap} = 5115 keV and E_{nn} = -7192 keV. For Z=9, 10, 11, 12, 13 and 14 we thus obtain E_{pn} = -1752, -3736, -3540, -3954, -2184 and -1222 keV, respectively. These turn out to be qualitatively similar to the "correlation" energy discussed by Poves and

Retamosa (Ref 27). However, a quantitative comparison cannot be made since the correlation energy is not itself quantitatively defined.

In summary, we find that there are three mechanisms which combine to give the inversion of $2\hbar\omega$ relative to $0\hbar\omega$: the (small) reduction in the ESPE gap, the pairing energy E_{nn}, and the proton-neutron interaction energy E_{pn}. The only one of which should have a strong Z dependence is E_{pn}.

For all N=Z nuclei in the sd shell, there are low-lying (1.4-2.2 MeV) collective 2^+ states. When both protons and neutrons fill the beginning of a major shell there are strong ^{4}He-type correlations which lead to well-defined prolate deformations as in the case of ^{20}Ne and ^{24}Mg in the sd shell. The prolateness of ^{20}Ne and ^{24}Mg is reinforced by the small energy gap between the $d_{5/2}$ and $s_{1/2}$ orbits in the lower part of the sd shell. In N=Z nuclei in the middle to end of a major shell there is a competition between prolate and oblate deformations as in the case of ^{28}Si, ^{32}S and ^{36}Ar in the sd shell. For these nuclei the type of collectivity is particularly sensitive to the spacing of the single-particle orbits in the major shell.

For the $2\hbar\omega$ configurations in N=20, we note that the two-neutron configuration will always tend toward collectivity because the $f_{7/2}$ and $p_{3/2}$ neutrons orbits are close for all Z values (see Fig. 4). However, the situation for the two-proton configuration is quite different. At N=20 and Z=8 the $d_{5/2}$ orbits and $s_{1/2}$ proton ESPE are close in energy (see Fig. 10), and this reinforces the collectively of the (neutron-pf)^2(proton-sd)^2 configuration near ^{28}O. Hence E_{pn} is large for ^{30}Ne. However, the gap between the $d_{5/2}$ and $s_{1/2}$ proton ESPE increases to about 6 MeV for ^{34}Si. In this case the $d_{5/2}$ protons tend to form a closed shell, and the energy of the $0\hbar\omega$ 2^+ state in ^{34}Si is very high (4.9 MeV). Thus, in the weak-coupling model the contribution to E_{pn} is greatly reduced and would be zero in the limit of a $(d_{5/2})^6$ proton closed-shell configuration (since only the monopole term can contribute in this case). This is the reason for the strong Z dependence in E_{pn} and for the end of the island of inversion in ^{34}Si. As a consequence of the large $d_{5/2}$-$s_{1/2}$ proton splitting in ^{34}Si, the $d_{5/2}$ proton truncation assumed by Poves and Retamosa may be partly useful for nuclei just below ^{34}Si (with some effective interaction changes), but closer to ^{28}O the explicit contribution from the proton $s_{1/2}$ orbit must be taken into account, and for the the Gamow-Teller decay properties the $d_{3/2}$ orbit will always be important.

The E_{nn} contribution to the $1\hbar\omega$ excitation energy in the N=19 nuclei can be estimated from ^{27}O as E_{nn} = Ex - E_{gap} = 2110-5115 keV = -2077 keV. E_{pn} as a function of Z is then about -1448, -1899, -1804, -2102, -1151, -1175 keV for ^{28}F, ^{29}Ne, ^{30}Na, ^{31}Mg, ^{32}Al and ^{33}Si, respectively. The results for the $1\hbar\omega$ states of the N=21 nuclei are E_{nn} = -4187 and E_{pn}(Z) = -304, -1837, -1736, -1862, -1033 and -47 for ^{30}F, ^{31}Ne, ^{32}Na, ^{33}Mg, ^{34}Al and ^{35}Si, respectively. The lowering of these states is due to the ^{3}He(^{3}H)-type correlation energy, and the relative magnitudes of these $E_{pn}(1\hbar\omega)$ relative to the $E_{pn}(2\hbar\omega)$ due to ^{4}He-type correlations discussed at the beginning of this section are reasonable. The inversion of the $2\hbar\omega$ excitations relative to $0\hbar\omega$ appears when the $0\hbar\omega$ is itself not very collective. The reason why there is not an inversion of the $3\hbar\omega$ relative to $1\hbar\omega$ in N=19 and 21 is probably because the $1\hbar\omega$ are themselves already fairly collective. For ^{31}Na we do find an inversion of $3\hbar\omega$ relative to $1\hbar\omega$.

It is well known that $n\hbar\omega$ spectra often lie very low in excitation energy for the reasons discussed above. The lowing lying $4\hbar\omega$ 4p-4h state in ^{16}O and its explanation in terms of a weak-coupling model (Ref 32) is perhaps the most famous example. In fact, if the p-sd single-particle gap were only about 1 MeV smaller than what is actually is, this would probably be the ground state of ^{16}O and the island of inversion near ^{31}Na would not be so unique. The same can be said of ^{40}Ca. But by the time we reach A=80 the nominal shell closure of the pf shell is lost by the lowering of the $g_{9/2}$ orbit, and beyond this point it is well known that magic numbers are no longer those of the major harmonic oscillator shells. The mechanisms behind our island of inversion are also responsible for the low-lying intruder states in heavy nuclei (Ref 33). This suggests obvious applications of the weak-coupling approximation to these heavy nuclei. Relationships to the deformed shell-model approach have also been pointed out (Ref 34). In addition, we note that there is a similar intruder state problem in the region around ^{12}Be, where the ground state of ^{11}Be has a well-known $1\hbar\omega$ $1/2^{+}$ configuration.

3.3 Comments on the comparisons to experiment

In Ref 5 we discuss many examples where the qualitative aspects of our weak-coupling calculations agree with experiment. Here we give a few examples and some comments on places where more experimental data are needed and/or where more calculations are needed.

a) The low excitation energy of both the $1\hbar\omega$ (Fig. 8) and $2\hbar\omega$ (Fig. 7) configurations in ^{31}Mg are consistent with the recent data which shows a large level density at low excitation energy (Ref 35). However, we are not able at present to calculate the precise order of these configurations or the order of the states within a given configuration. We note that ^{31}Al has experimental β decay properties as well as low-lying levels which agree with the the sd calculation, but that ^{31}Mg has experimental β decay properties which are in complete disagreement with the sd calculation (Ref 36). This indicates that the ground state of ^{31}Mg is not the expected $3/2^+$ sd configuration, but is a $1\hbar\omega$ or $2\hbar\omega$ configuration. More experiments and calculations are needed to sort out the possibilities.

b) In ^{34}Si, the 2^+ state seen experimentally at 3.33 MeV is close to where we would expect our 2^+ $2\hbar\omega$ state. The negative parity states near 4.3 MeV are close to where we predict the $1\hbar\omega$ excitations to start (see Fig. 8) and are also consistent with the β decay of ^{34}Al (Ref 30). The Poves-Retamosa calculations are also in reasonable agreement for these known states (Ref 37). However, we predict a 0^+ state from the $2\hbar\omega$ configuration around 1.5 MeV (see Fig. 7), whereas the Poves-Retamosa calculation puts this excited 0^+ state near 4 MeV (Ref 37). This state has not yet been observed experimentally.

c) In ^{32}Mg the known 2^+ state at 0.88 MeV is close to where we expect the first excited state of the $2\hbar\omega$ ground-state band. Because the $1\hbar\omega$ and $2\hbar\omega$ configurations in ^{32}Na are close in energy (and both below the $0\hbar\omega$ configuration) the states around 3.0 MeV in ^{32}Mg seen in the ^{32}Na β decay have several interpretations in our model. If ^{32}Na has a $2\hbar\omega$ ground state then it would have a negative parity and would decay to the negative-parity states expected around 3 MeV in ^{32}Mg. If ^{32}Na has a $1\hbar\omega$ ground state we predict that this would be 0^+ and then it would decay to 1^+ states in ^{32}Mg which could also lie around 3 MeV (we have not yet made calculations for these 1^+ states). The excitation energy in ^{32}Mg of our predicted 0^+ state from the $0\hbar\omega$ configuration is around 1 MeV (see Fig. 7). In contrast, the Poves-Retamosa calculations predict a 4^+ state at about this excitation energy. More experimental information is needed to test these predictions.

d) The most serious disagreement with our present calculations is the underbinding of ^{32}Na and ^{33}Na. Even though our intruder states comes below the

$0\hbar\omega$ configurations (see Figs. 7 and 8) for these nuclei, it is not enough to explain the magnitude of the discrepancy indicated in Fig. 5. It would be very useful to have new experimental data for the masses of the neutron rich Ne and Na isotopes. Continued disagreement with experiment may indicate, for example, that our extrapolated pf single-particle energies are wrong.

e) For the secondary-beam experiments which may eventually be possible, we would like to suggest that one-nucleon transfer experiments will provide the most valuable spectroscopic information for improving the calculations. Theoretical extrapolations of the single-particle energies in nuclei far from stability are difficult and uncertain. They are also the most important single ingredient for the understanding of more detailed aspects of the structure.

f) Calculations are needed for the β-decay properties of the intruder states. In particular, the unusual half-life and decay properties of ^{31}Mg (Ref 36) must be understood.

4. BETA DECAY PROPERTIES

Beta decay and electromagnetic properties provide exacting tests of the wavefunctions. For the nuclei close to stability the $0\hbar\omega$ shell-model calculations have been well tested. In the sd shell essentially all data have been compared for Gamow-Teller β decay (Ref 38), M1 gamma decay and μ moments (Ref 39 and Ref 40), E2 gamma decay and Q moments (Ref 2 and Ref 41). With simple effective operators, the comparison between experiment and theory is excellent. For the half-life and Gamow-Teller strength functions discussed below, the most important aspect of the effective operator from the known sd-shell data is the overall quenching factor of about 0.60 in the B(GT) values (Ref 40). (That is, the experimental B(GT) values are 60% of that expected theoretically.) There are some orbit and mass dependences found and expected in the effective Gamow-Teller operator (Ref 40). In particular, one does not expect so much quenching for the p-shell nuclei. However, for uniformity we include this overall quenching factor of 0.60 in all the comparisons for exotic nuclei discussed below.

4.1 Neutron-rich sd model space

In conjunction with our study of individual Gamow-Teller matrix elements near the N=Z line (Ref 38), we calculated the half-lives and final-state branching ratios for all neutron rich sd-shell nuclei (Ref 36). The half-life

comparison is shown in Fig. 11 for an older set of data (Ref 36 and Ref 42). The new half-lives measured since we published these predictions (Ref 43, Ref 44, Ref 45 and Ref 46) are in reasonable agreement. The major disagreement in the half-life and decay of ^{31}Mg noted in Ref 38 still stands and was discussed in terms of the intruder states in the last section.

Several new data have appeared on the details of the final state gamma-decay spectra seen in these β decay. The decay of ^{22}O has been studied and compared with the sd-shell calculations (Ref 43). These data when combined with the transfer data (Ref 47) provide a spectrum for ^{22}F which is in excellent agreement with the calculations. [The apparent disagreement between excitations energies obtained from transfer reactions (Ref 48) and β decay has been attributed to doublet structure of the ^{22}F ground state (Ref 43 and Ref 47)]. For the β branching, it is particularly interesting to note that the decay to the lowest 1^+ state is predicted to be very weak. It is also weak in the experiment but perhaps not as much so as predicted. In the extreme j-j coupling picture we would expect the lowest 1^+ states to have a $d_{5/2}$ proton-particle neutron-hole configuration and to have a reasonably large strength. Its counterpart in the the pf shell is well known as the lowest 1^+ state in ^{48}Sc and is strong in the ^{48}Ca(p,n) reaction (Ref 49). In contrast, the simple particle-hole state in ^{22}F is the second state at 2.37 MeV in the calculation and the lowest 1^+ state has a completely different nature. This state turns out to have a strong overlap with the ^{20}O + dueteron configuration.

The recent detailed study of the ^{29}Na (Ref 50) and ^{30}Na (Ref 51) β decays provides much new information on the Gamow-Teller strength functions and the final state spectra which are in reasonable agreement with the sd-shell calculations. The quenching observed for ^{29}Na is consistent with the 0.6 factor discussed above, but the quenching observed for ^{30}Na is about a factor of two larger (that is, the theory has to be multiplied by a factor of about 0.3 rather than 0.6). Again, this may relate to the intruder state problem (Ref 51). Beta decay calculations including the intruder states for these nuclei have not yet been carried out. Alternatively, it may indicate that the Gamow-Teller strength function is systematically moved to a higher energy compared to the calculation.

Qualitative aspects of the calculated beta delayed neutron probabilities can be inferred from the tables in Ref 36. (In some cases there is the possibil-

ity that not enough excited states were calculated for the tabulations of Ref 36. However, in the following examples this is not the case.) For example, a Pn value of 1.9% for ^{23}O can be obtained by assuming that all beta decays to levels above the neutron-decay threshold in ^{23}F of 7.55 MeV will neutron decay. (The two-neutron decay threshold of 12.74 MeV is above the beta-decay Q value of 11.63 MeV.) This is in disagreement with a recent experimental result of Pn = 31±7% (Ref 46). Similarly, for ^{24}O the calculated Pn of 15.3%, obtained with a neutron decay threshold of (3.9±0.2) MeV for ^{24}F (Ref 22), is in disagreement with the experimental value of 58±12% (Ref 46). (Since a level at 4.1 MeV in ^{24}F accounts for 10% of this Pn value, the Pn would be reduced to 5.3% if this level turned out to be below the neutron-decay threshold.) It is not clear to us why these disagreements are so large.

4.2 Neutron-rich p-sd and sd-pf model spaces

Calculations and comparison to experiment for the half-lives and branching ratios have also been made for neutron-rich p-sd nuclei (Ref 45, Ref 52, Ref 53, Ref 54 and Ref 55) and sd-pf nuclei (Ref 29). The parent nuclei are assumed to have $0\hbar\omega$ ground state configurations and then the GT leads to $1\hbar\omega$ excited state configurations in the daughter nucleus. The decay to the lower-lying $0\hbar\omega$ states in the daughter nuclei is first-forbidden. Except in unusual circumstances, the first-forbidden branchings are negligibly small in these two mass regions (Ref 55) and have been ignored in some calculations (Ref 52 and Ref 53).

For both the p-sd and sd-pf regions the calculated half-lives are within about a factor of two of those measured. In particular, as we mentioned in Ref 53, the experimental half-lives for ^{11}Li and ^{12}Be are about a factor of two larger than those calculated, giving some hint of intruder state mixing. As was mentioned above for the binding energies in the region, the calculations could probably be improved with a better effective interaction. It would also be interesting to investigate the intruder state problem in the region around ^{12}Be. In the future we plan to extract the delayed neutron probabilities from the Gamow-Teller strength functions calculated in the p-sd region in order to compare with experiment (Ref 45, Ref 46, and Ref 54). In the sd-pf region, in addition to the theoretical work mentioned above which needs to be done, it is important for the element synthesis aspects of astrophysics to extend the beta-decay calculations to the region of $16 \leq Z \leq 20$ and $22 \leq N \leq 30$.

4.3 Proton-rich sd model space

Data on the proton-rich side of the sd shell provides complimentary information to that obtained on the neutron-rich side. Because of the Coulomb interaction the stable nuclei do not extend out so far in |N-Z| as on the neutron rich side, but beta decay Q values are larger allowing for study of the Gamow-Teller strength function up to and just above the isobaric analogue state. The proton-rich stable nuclei do not extend far enough in |N-Z| to run into the intruder state problem observed on the neutron-rich side. Recent experiments have probably reached the limit of stability on the proton-rich side (Ref 56 and Ref 57) and delayed proton spectra have been or are currently being analyzed for most of these (Ref 56 and Ref 58).

The half-lives of the proton-rich nuclei are in excellent agreement with theory (Ref 59 and Ref 60). Experimental determination of the complete Gamow-Teller strength functions requires a complex analysis of all delayed gammas and protons. Several of these cases for T_z=-1 and T_z=-3/2 were included in the analysis of Ref 38. In the few more recent cases, those of ^{32}Ar and ^{33}Ar (Ref 61) where such a complete analysis has been carried out, the agreement with the sd-shell theory is good.

It turns out that the Q value for these β^+ decays allows for measurable transitions to final states only up to about the middle of the Gamow-Teller strength function in the Cl nuclei. Thus, the comparison between experiment and theory is sensitive to the energy of the Gamow-Teller resonance. It is difficult to distinguish between energy shift effects and quenching when only part of the Gamow-Teller strength function can be measured. This comment applies generally to all β^+ and β^- decays discussed here (see the comment above concerning the ^{30}Na decay.)

In many cases there is experimental information only on the delayed protons. One thing one learns is the energy of the isobaric analoque state. This can then be combined with the masses of the other members of the isobaric multiplet to test and study the isobaric mass multiplet equation (IMME). Recently isospin nonconservation (INC) has been put into the sd-shell calculations with the result that one can calculate the coefficients of the IMME and compare to experiment. The comparison is good expecially for the "c" coefficients (Ref 60 and Ref 62).

The delayed proton spectra are complicated. The protons often go to intermediate states which themselves can proton decay so that one has to sum over a large number of intermediate states. Furthermore, the delayed protons from the isobaric analoque state are all isospin forbidden so that one must use an INC interaction to carry out the calculation. All of these calculations are now possible but time consuming. Such calculations for the decay of ^{28}S were in reasonable agreement with experiment (Ref 60). For the proton rich p and p-sd regions there can also be beta delayed ^{3}He and ^{4}He emission which are complicated because cluster overlaps have to be considered. However, we have made such calculations for the decay of ^{9}C (Ref 63) which are not inconsistent with the experimental data.

An interesting aspect in the combination of neutron and proton rich data is observation of mirror asymmetry in Gamow-Teller transitions. These provide limits on "second-class currents" in the weak interaction, after corrections for the standard INC nuclear structure effects are taken into account (Ref 64).

5. LARGE RADII AND COULOMB BREAK-UP CROSS SECTIONS

One of the first reaction studies with exotic beams was to measure the reaction cross sections on light stable targets (Ref 65 and Ref 66). The relatively large reaction cross section found for the most neutron-rich nuclei has been interpreted in terms of a extended matter (neutron) density for these nuclei (Ref 65) which is not easy to understand in terms of conventional Hartree-Fock calculations (Ref 67). This has lead to a number of less conventional models, such as the dineutron model (Ref 68), being proposed. We were thus lead to examine more carefully the assumptions which go into the more standard calculations (Ref 69).

We carried out a new set of calculations for the total cross sections with the following assumptions:

a) The radial wave functions were obtained from standard Hartree-Fock calculations using the SGII Skyrme-type interaction (Ref 3).

b) The orbit occupancies were constrained by the type of $0\hbar\omega$ shell-model calculations described above (expect for the ground state of ^{11}Be for which a $1\hbar\omega$ shell-model space was used.)

c) The binding energy of the last neutron orbit was constrained to reproduce either: (i) the one-neutron separation energy in the case of a closed neutron shell (e.g. ^{11}Li and ^{12}Be) or a single valence neutron (e.g.^{11}Be), or (ii) one-half of the two-neutron separation energy in the case where two-neutrons are in the valence shell (e.g. ^{14}Be.) These binding energies were constrained by multiplying the central part of the Hartree-Fock potential by a constant.

d) A Glauber-type model using a zero-range and a finite range nucleon-nucleon interaction with cross section parameters of σ_{nn} = 40mb was then used to calculate the cross sections. The results are compared to experiment in Fig. 12.

The general trend of the experiment is well reproduced by the calculation. The key ingredient in getting the cross section trend correct is in fixing the binding energy of the valence neutron as described in (c) above. The potential normalizations of 0.82 to 0.86 which were required are not unrealistic. They reflect the uncertainties introduced from reducing the many-body problem to a mean-field problem and by using a Skyrme-type interaction adjusted to properties of nuclei near the valley of stability. Of course it would be better to have a more fundamental approach. But we believe that our calculations reflect the essential physics of the situation.

More recently the reaction cross section experiments were extended to heavy stable targets (Ref 70). The Z and A dependence of the total and partial cross sections were then used to infer the amount due to Coulomb excitation and subsequent breakup. The inferred cross sections for this Coulomb-excitation process turned out to be surprisingly large and has lead one to speculate on the existence of a low-lying "soft-giant dipole state" (Ref 70). It is important to study what is expected from conventional nuclei structure models, and we will make a few comments in this regard on ^{11}Be and ^{11}Li.

The structure of ^{11}Be is thought to be relatively well understood. The $1/2^+$ ground state is, in fact, a $1\hbar\omega$ intruder state of the type discussed above for the sd-pf region. The only other bound state is the $1/2^-$ state at 0.32 MeV which is associated with the $0\hbar\omega$ p-shell configuration. The low-lying nature of the $1/2^+$ state can be qualitatively understood in terms of the weak-coupling model discussed above or in terms of the Nilsson model. The low-lying spectrum of ^{11}Be is also easy to reproduce in a $0\hbar\omega$ plus $1\hbar\omega$ shell-model calculation (Ref 11 and Ref 71). The $1/2^+$ to $1/2^-$ E1 transition, with

a B(E1) = 0.12 e^2fm^2 = 0.36 W.u., is one of the strongest known between bound states (Ref 71). The theoretical value is very sensitive to the radial wave functions used. But the experimental B(E1) value can be reproduced if the radial wavefunctions are generated from potentials which reproduce the experimental separation energies (Ref 71). In the calculation, the only other E1 transition of the type $1\hbar\omega$ to $0\hbar\omega$ is to an unbound $3/2^-$ state at 3 MeV in excitation. The calculated $1/2^+$ to $3/2^-$ B(E1) is again about 0.13 e^2fm^2. However, this is over an order of magnitude too small to account for the inferred experimental Coulomb excitation cross section on Pb of 0.6 to 1.0 bn (Ref 72). The remaining E1 strength lies in the $1\hbar\omega$ (ground state) to $2\hbar\omega$ transitions, and preliminary shell-model calculations in this space put most of the dipole strength above 10 MeV in excitation, which is much too high in energy to account for the experimental cross section.

Bertsch and Foxwell have recently examined the case of ^{11}Li in the framework of the RPA model (Ref 73). The method used takes into account the continuum aspects of the problem (Ref 74) which is important in describing the E1 strength down to the neutron decay threshold. The experimental magnetic moment and $3/2^-$ spin value confirm the expected valence $p_{3/2}$ proton configuration (Ref 75) for this nucleus. However, the neutron structure of the ^{11}Li ground state may not be well understood. The neutrons may have a $0\hbar\omega$ closed shell configuration with the valence nucleons in the p shell (as was assumed above for the total reaction cross section calculations), or they may have a some $(sd)^2$ configuration from the intruder state, or something in between. (A measurement of the quadrupole moment would be sensitive to the deformation and hence more sensitive to the neutron configuration.) With the same assumptions that went into the total cross section calculations described above (a $p_{1/2}$ valence configuration with a 1.0 MeV binding energy), the cross section for calculated for ^{11}Li on Pb was 0.19 bn - much smaller than the value of $>0.9\pm0.1$ bn inferred from experiment (Ref 70). In the extreme case where the the valence neutrons were assumed to be in the $s_{1/2}$ orbit with a small separation energy of 0.19 MeV a cross section of 0.54 bn was obtained - still smaller than experiment.

Thus, in summary, it seems that the large Coulomb excitation cross sections inferred from experiment are difficult to understand in a conventional approach. There is, however, some model dependence in subtracting the nuclear part of the interaction to obtain the Coulomb excitation cross section

and this should be examined more carefully. A consistent calculation should be able to reproduce the total and partial cross sections as well as the momentum distributions of the fragments (Ref 76), and there is more work to be done.

Acknowledgements: This work was supported in part by the US National Science Foundation grant number PHY 87-14432.

FIGURE 1

Binding energies of states of the He isotopes (Ref 14). The experimental energies are shown by circles and experimental ground-state binding energies are connected by a line. The calculated energies are shown by the crosses (slightly offset to the right in the case when they are close to the circles).

FIGURE 2

Binding energies of the ground states of the O isotopes. (a) The experimental energies (solid circles) are compared to three calculations (solid lines) discussed in the text: Moeller-Nix (MN), W-sd for N$\leq$20 plus W-MG-WBMB-sd-pf for N$\geq$20 (W), and SDPOTA-sd (A). For display 10 MeV has been added to the W comparison and 20 MeV has been added to the A comparison. (b) An expanded version of (a) showing the region near the stability line. For display 5 MeV has been added to the W comparison and 10 MeV has been added to the A comparison.

FIGURE 3

Neutron single-particle energies for the O isotopes (Z=8) as a function of neutron number. The values at N=14 and 16 were obtained in the extreme j-j coupling limit.

FIGURE 4

Neutron single-particle energies for the N=20 isotones as a function of proton number. The values at Z=14 and 16 were obtained in the extreme j-j coupling limit.

FIGURE 5

Difference between the measured and calculated binding energies for the sd and sd-pf regions. The calculation is W-sd for N$\leq$20 and W-MG-WBMB-sd-pf for N$\geq$20. The lines indicate the semi-magic numbers N=14 and 16 and the zero for the Na and Mg isotope differences.

FIGURE 6

Comparison of experimental and theoretical levels in ^{27}Al from Lickert et al. (Ref 23). For each spin, the numbers label the energy in keV for the experimental levels on the left-hand side which are connected by a dashed

line to the associated theoretical levels on the right-hand side.

FIGURE 7

Neutron-rich nuclei in the A=32 region. The listed numbers are the predicted excitation energies (in keV) of the $2\hbar\omega$ ground state relative to the $0\hbar\omega$ ground state, $E_x(2\hbar\omega)$. The symbols denote weak-coupling, W, the full W-MG-WBMB-sd-pf model space, F, and a truncated version of this model space, T (not discussed in the text). We label the excitation energies beyond our computational resources with asterisks and, for these cases, show the J-dimension of the N+2 isotope necessary to provide the weak-coupling (W) prediction. The magic numbers Z=8 and N=20 are emphasized with double lines.

FIGURE 8

Neutron-rich nuclei in the A=32 region. The top two listed numbers are the $E_x(1\hbar\omega)$ in keV for weak-coupling, W, and the full W-MG-WBMB-sd-pf model space, F. The bottom number is $E_x(3\hbar\omega)$ for weak-coupling. We label the excitation energies beyond our computational resources with asterisks. The magic numbers Z=8 and N=20 are emphasized with double lines.

FIGURE 9

Partial periodic table highlighting the "island of inversion" centered at ^{32}Na. The magic numbers Z=8 and N=20 are emphasized with double lines.

FIGURE 10

Proton single-particle energies for the N=20 isotones as a function of proton number. The values at Z=14 and 16 were obtained in the extreme j-j coupling limit.

FIGURE 11

Comparison of half-lives calculated for the Gamow-Teller beta decay of sd-shell nuclei with five of more excess neutrons with experimental data (Ref 36). Experimental data from Ref 42 are shown as squares and other experimental data summarized in Ref 36 are shown as triangles. The calculated values are connected by the solid lines. Newer data from Ref 43, Ref 44, Ref 45 and Ref 46 not shown are in reasonable agreement with the calculations.

FIGURE 12

(a) The reaction cross sections for the Li isotopes on a ^{12}C target (Ref 69). The solid line connecting the boxes (circles) shows the theoretical cross sections obtained with the finite-range interaction (zero-range interaction) version of the Glauber model calculations. The nucleon-nucleon cross section parameter is taken as 40 mb. The data are taken from Ref 65. (b) Same as in (a) but for the Be isotopes.

References

1. A. de-Shalit and I. Talmi, Nuclear Shell Theory, (Academic Press, 1963).
2. B. A. Brown and B. H. Wildenthal, Ann. Rev. of Nucl. and Part. Sci. 38, 29 (1988).
3. Nguyen van Giai and H. Sagawa, Phys. Lett. 106B, 379 (1981).
4. B. A. Brown, Workshop on Microscopic Models in Nuclear Structure Physics, (World Scientific, 1989) pp. 337-355.
5. E. K. Warburton, J. A. Becker and B. A. Brown, Phys. Rev. C, to be published.
6. S. Cohen and D. Kurath, Nucl. Phys. 73, 1 (1965), Nucl. Phys. A101, 1 (1967).
7. D. J. Millener, private communication.
8. B. H. Wildenthal, Progress in Particle and Nuclear Physics 11, edited by D. H. Wilkinson (Pergamon, Oxford, 1984) p. 5.
9. B. A. Brown, W. A. Richter, R. E. Julies and B. H. Wildenthal, Ann. Phys. 182, 191 (1988).
10. J. B. McGrory, Phys. Rev. C8, 693 (1973).
11. N. Poppelier, L. D. Wood and P. W. M. Glaudemans, Phys. Lett. B157, 120 (1985) and N. Poppelier, Thesis, Univ. of Utrect, 1989.
12. D. J. Millener and D. Kurath, Nucl. Phys. A255, 315 (1975).
13. E. K. Warburton, J. A. Becker, D. J. Millener and B. A. Brown, BNL Report 40890 (1987).
14. J. Stevenson et al., Phys. Rev. C37, 2220 (1988).
15. K. K. Seth et al., Phys. Rev. Lett. 58, 1930 (1987).
16. D. Guillemaud-Mueller et al., Phys. Rev. C, to be published.
17. M. Langevin et al., Phys. Lett. 150B, 71 (1985); F. Poughoen et al., Europhys. Lett. 2, 505 (1986).
18. C. Detraz and D. J. Vieira, Ann. Rev. of Nucl. Part. Phys. 39, 407 (1989).

19. D. J. Vieira and J. M. Wouters, AIP Conference proceedings 164, 1 (1988).

20. P. Moeller and J. J. Nix, At. Data Nucl. Data Tables 39, 231 (1988).

21. A. H. Wapstra, G. Audi and R. Hoekstra, At. Data Nucl. Data Tables 39, 281 (1988).

22. D. J. Vieira et al., Phys. Rev. Lett. 57, 3253 (1986); A. Gillibert et al., Phys. Lett. 192B, 39 (1987).

23. M. Lickert et al., Z. Phys. A331, 409 (1988).

24. C. Thibault et al., Phys. Rev. C12, 644 (1975); C. Detraz et al., Nucl. Phys. A394, 378 (1983); C. Detraz et al., Phys. Rev. C19, 164 (1979).

25. B. H. Wildenthal and W. Chung, Phys. Rev. C19, 164 (1979).

26. X. Campi et al., Nucl. Phys. A251, 193 (1975).

27. A. Poves and J. Retamosa, Phys. Lett. B184 311 (1987).

28. M. H. Storm, A. Watt and R. R. Whitehead, J. Phys. G9, L165 (1983); A. Watt, R. P. Singhal, M. H. Storm and R. R. Whitehead, J. Phys. G7, L145 (1981).

29. E. K. Warburton et al., Phys. Rev. C34, 1031 (1986); J. W. Olness et al., Phys. Rev. C34, 2049 (1986); E. K. Warburton, Phys. Rev. C35, 2278 (1987); E. K. Warburton, J. A. Becker, B. A. Brown and D. J. Millener, Ann. Phys. 187, 471 (1988); E. K. Warburton and J. A. Becker, Phys. Rev. C35, 1851 (1987); Phys. Rev. C39, 1535 (1989); Phys. Rev. C40, 2823 (1989).

30. E. K. Warburton and J. A. Becker, Phys. Rev. C37, 754 (1988).

31. R. D. Lawson, Theory of the Nuclear Shell Model , (Clarendon Press, Oxford, 1980).

32. L. Zamick, Phys. Lett. 19, 580 (1965).

33. K. Heyde et al., Physics Reports 102, 291 (1983); Phys. Rev. C38, 984 (1984); Nucl. Phys. A466, 189 (1987); Nucl. Phys. A484, 275 (1988)

34. K. Heyde et al., Phys. Lett. 218B, 298 (1989).

35. P. Baumann et al., unpublished.

36. B. H. Wildenthal, M. S. Curtin and B. A. Brown, Phys. Rev. C28, 1343 (1983).

37. P. Baumann et al., Phys. Lett. 228B, 458 (1989).

38. B. A. Brown and B. H. Wildenthal, At. Data Nucl. Data Tables 33 (1986) 347.

39. M. C. Etchegoyen, A. Etchegoyen, B. H. Wildenthal, B. A. Brown and J. Keinonen, Phys. Rev. C38 (1988) 1382 (1988).

40. B. A. Brown and B. H. Wildenthal, Nucl. Phys. A474, 290 (1987).

41. M. Carchidi, B. H. Wildenthal and B. A. Brown, Phys. Rev. C34 (1986) 2280.

42. M. J. Murphy et al., Phys. Rev. Lett. 49, 455 (1982).

43. F. Hubert et al., Z. Phys. A333, 237 (1989).

44. J. P. Dufour et al., Z. Phys. A324, 487 (1988)

45. D. J. Vieira, private communication.

46. A. C. Mueller et al., preprint (IPNO-DRE-89-50) (1989).

47. N. A. Orr et al., Nucl. Phys. A491, 457 (1989).

48. N. M. Clarke et al., J. Phys. G14, 1399 (1988).

49. B. D. Anderson et al., Phys. Rev. C31, 1161 (1985).

50. P. Baumann et al., Phys. Rev. C36, 765 (1987).

51. P. Baumann et al., Phys. Rev. C39, 626 (1989).

52. M. Samuel et al., Phys. Rev. C37, 1314 (1988).

53. M. S. Curtin et al., Phys. Rev. Lett. 56, 34 (1986).

54. M. Lewitowicz et al., Nucl. Phys. A496 (1989).

55. E. K. Warburton, Phys. Rev. C38, 935 (1988) and E. K. Warburton and D. J. Millener, Phys. Rev. C39, 1120 (1989).

56. J. Aystro and J. Cerny, in Treatsie on Heavy-Ion Science, Vol 8, edited by D. A. Bromley.

57. M. Langevin et al., Nucl. Phys. A455, 149 (1986); M. G. Saint-Laurant et al., Phys. Rev. Lett. 59 (1987).

58. V. Borrel et al., preprint (IPNO-DRE-87-18) (1987) and private communication.

59. B. A. Brown and B. H. Wildenthal, unpublished.

60. F. Pougheon et al., Nucl. Phys. A500, 287 (1989).

61. Bjornstad et al., Nucl. Phys. A443, 283 (1985); M. J. G. Borge et al., Phys. Scr. 36, 218 (1987).

62. W. E. Ormand and B. A. Brown, Nucl. Phys. A440, 274 (1985); Nucl. Phys. A491, 1 (1989).

63. D. Mikolas et al., Phys. Rev. C37, 766 (1988).

64. I. S. Towner, Nucl. Phys. A216, 589 (1973).

65. I. Tanihata et al., Phys. Rev. Lett. 55, 2676 (1985); Phys. Lett. 160B, 380 (1985); and unpublished.

66. W. Mittig et al., Phys. Rev. Lett. 59, 1889 (1987).

67. H. Sata and Y. Okuhara, Phys. Lett. 162B, 217 (1985).

68. P. G. Hansen and B. Jonson, Europhys. Lett. 4, 409 (1987).

69. G. F. Bertsch, B. A. Brown and H. Sagawa, Phys. Rev. C39, 1154 (1989).

70. T. Kobayashi et al., Phys. Lett. B232, 51 (1989).

71. D. J. Millener et al., Phys. Rev. C28, 497 (1983).

72. T. Kobayashi et al., Proceedings of the International Nuclear Physics Conference - Abstracts, Sao Paolo Brazil, 1989.

73. G. F. Bertsch and J. Foxwell, preprint (1989).

74. S. Shlomo and G. Bertsch, Nucl. Phys. A243, 507 (1975); and G. Bertsch, "Computational Nuclear Physics", to be published by Springer, (1989).

75. E. Arnold et al., Phys. Lett. B197, 311 (1987).

76. T. Kobayashi et al., Phys. Rev. Lett. 60, 2599 (1988).

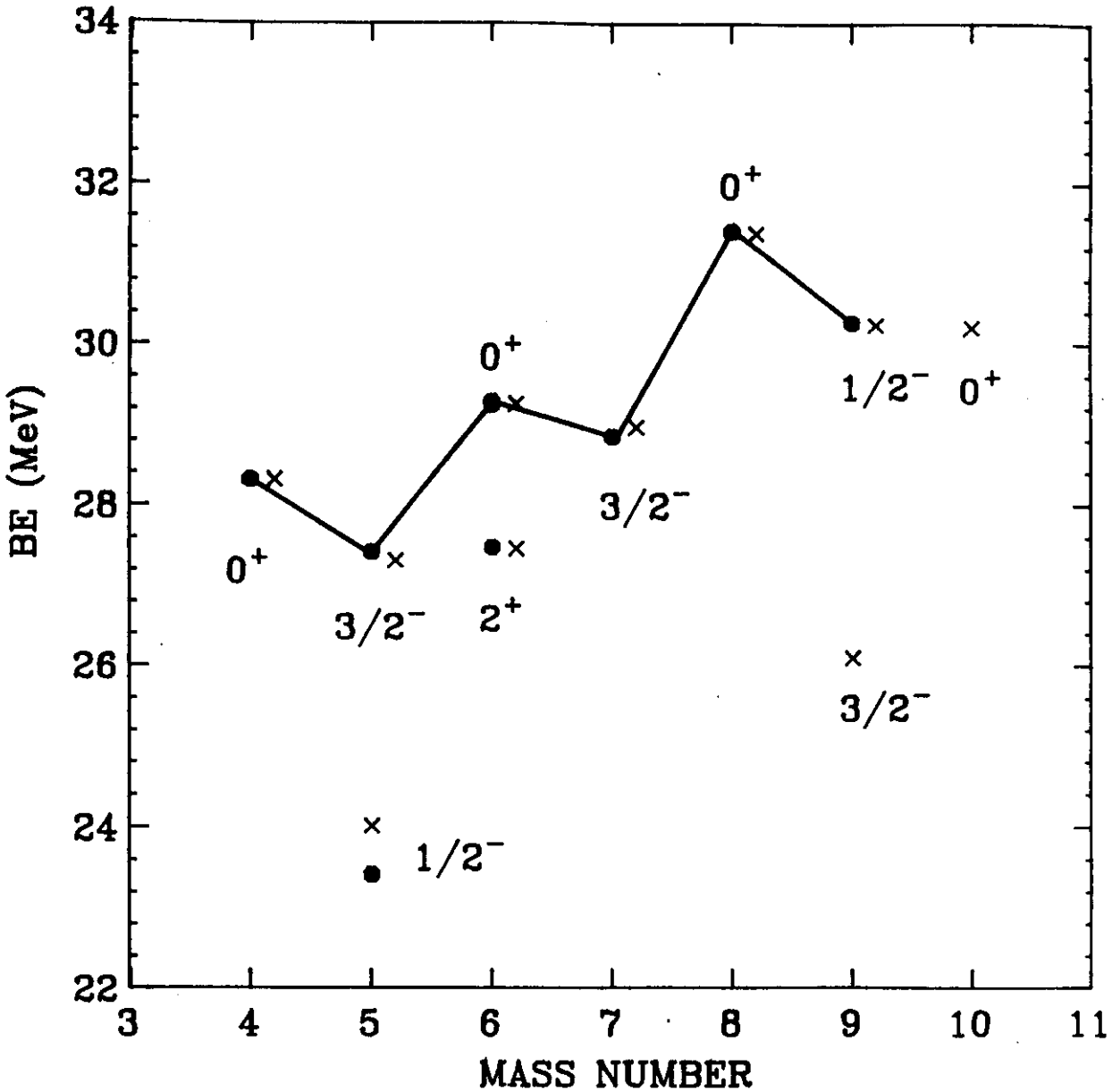
34
32
30
28
26
24
22
BE (MeV)
3
4
5
6
7
8
9
10
11
MASS NUMBER
0+
3/2−
0+
2+
3/2−
0+
1/2−
0+
3/2−
1/2−

FIGURE 1

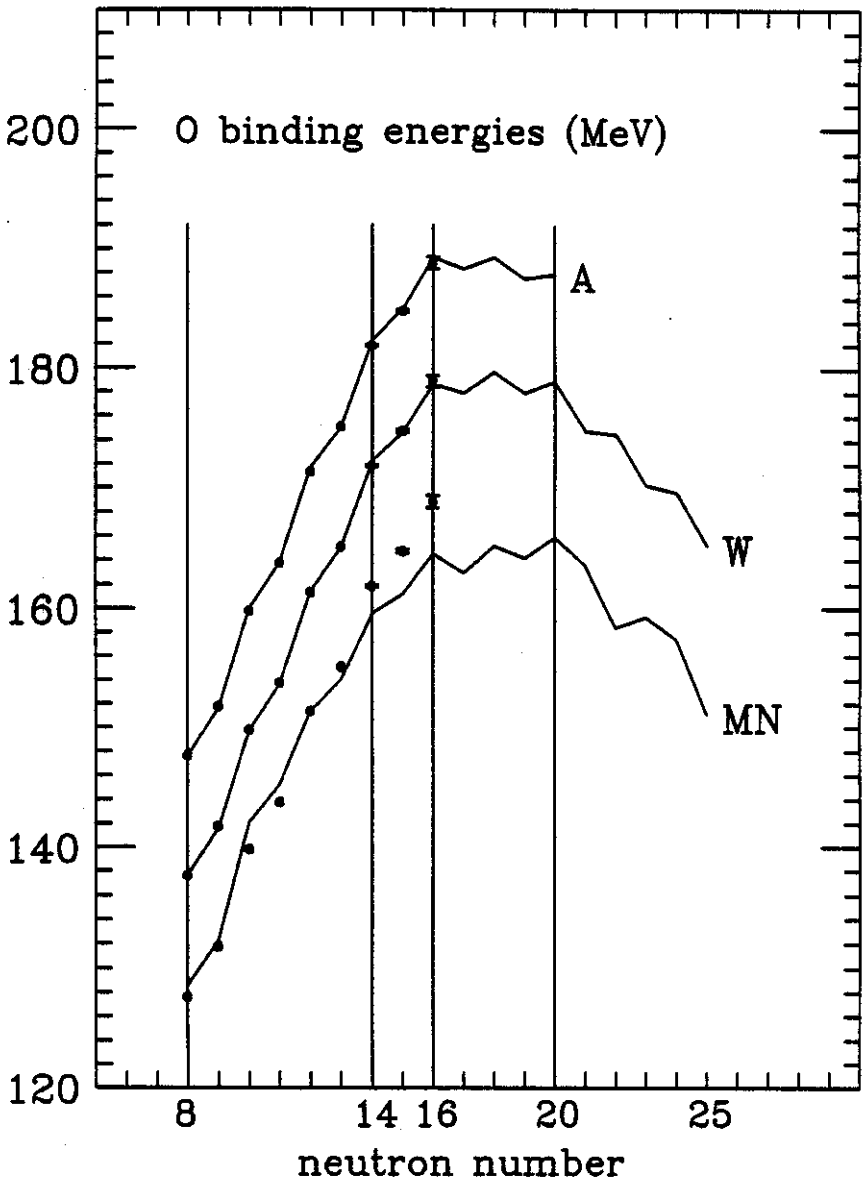
O binding energies (MeV)
200
180
160
140
120
A
W
MN
8
14 16
20
25
neutron number

FIGURE 2a

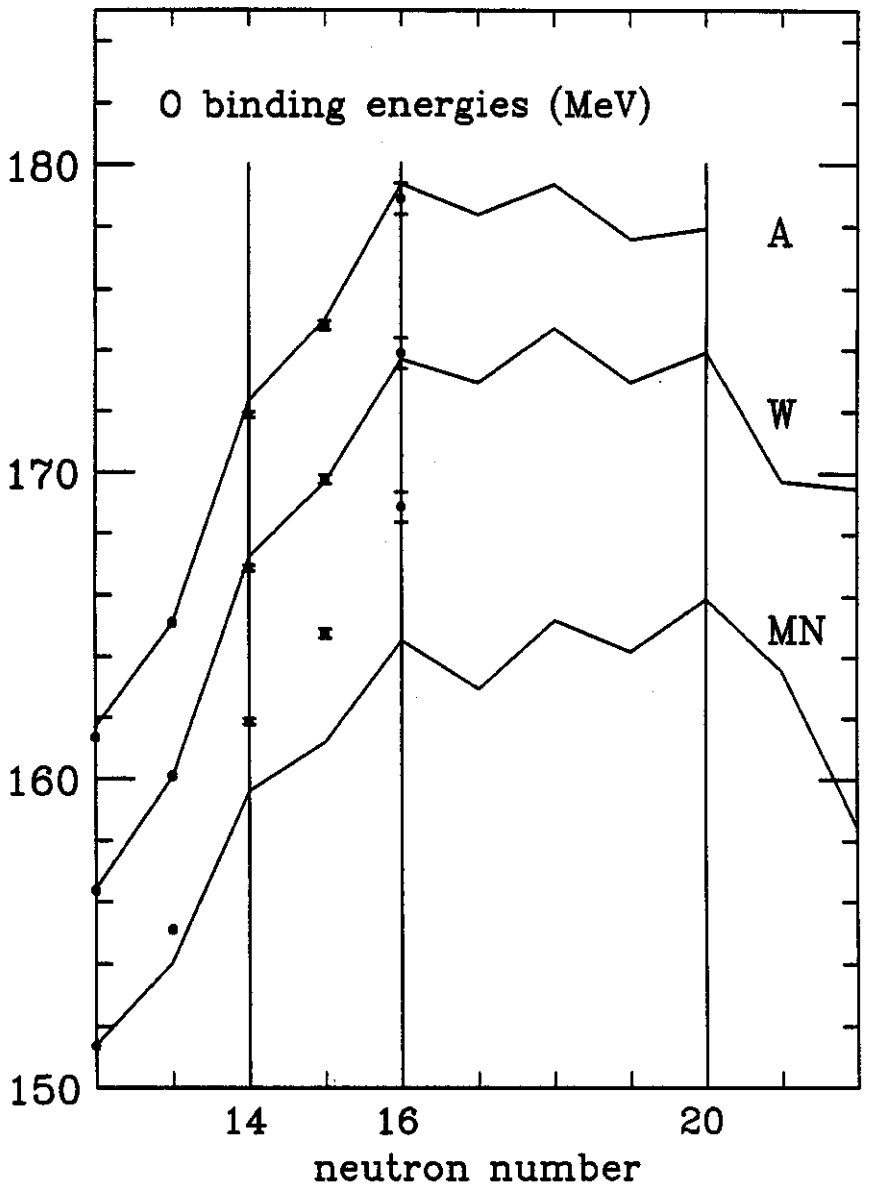
O binding energies (MeV)
180
170
160
150
A
W
MN
14
16
20
neutron number

FIGURE 2b

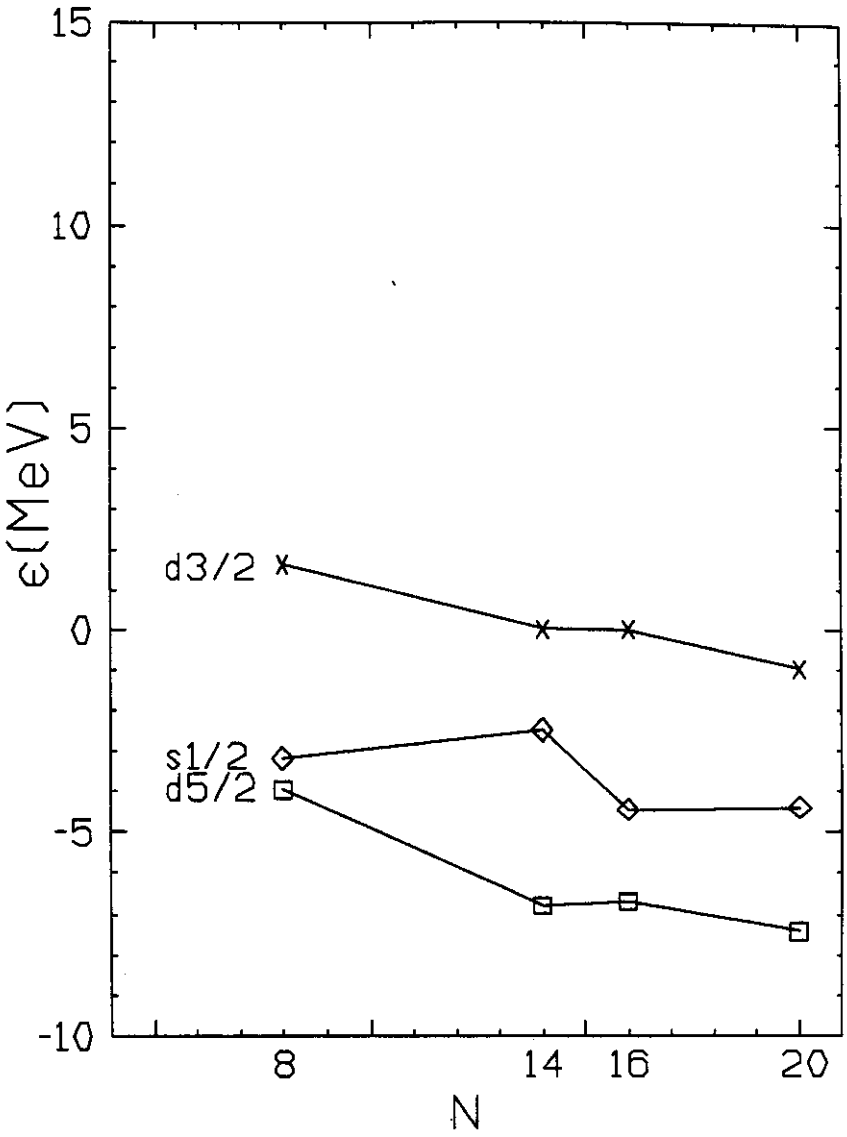

FIGURE 3

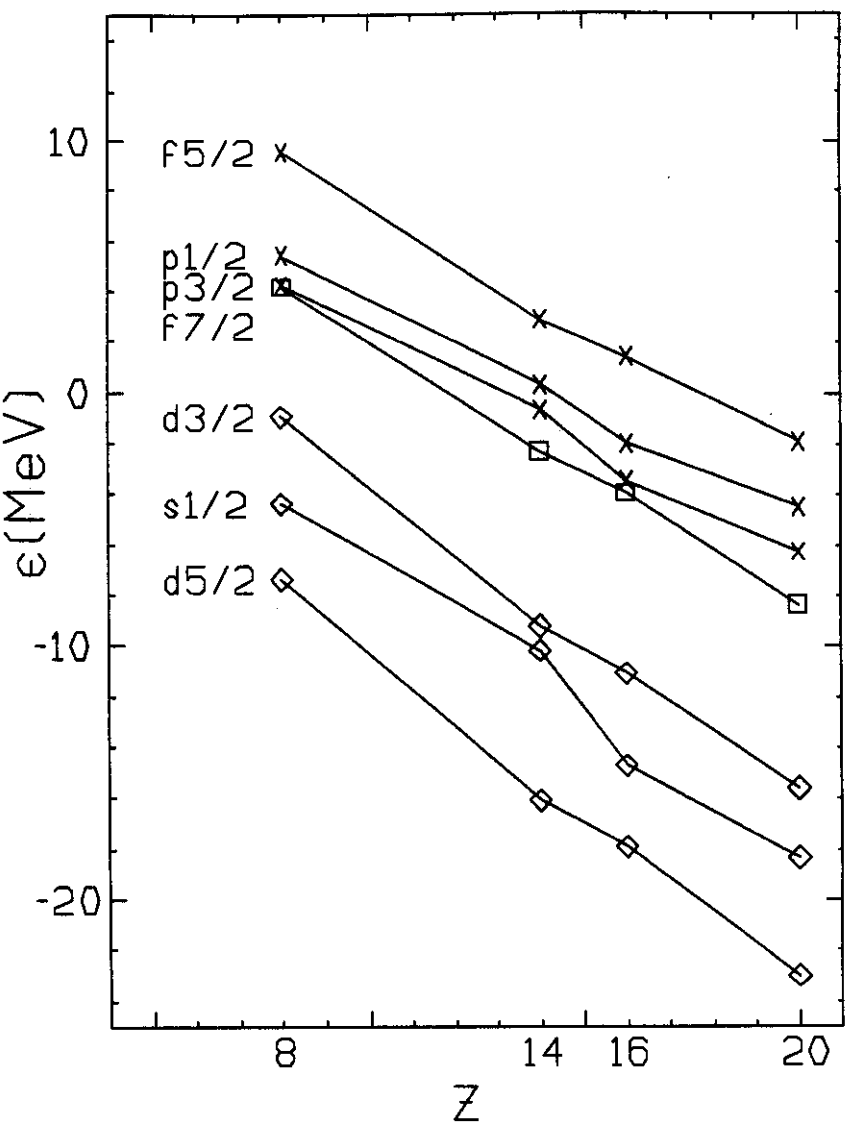

FIGURE 4

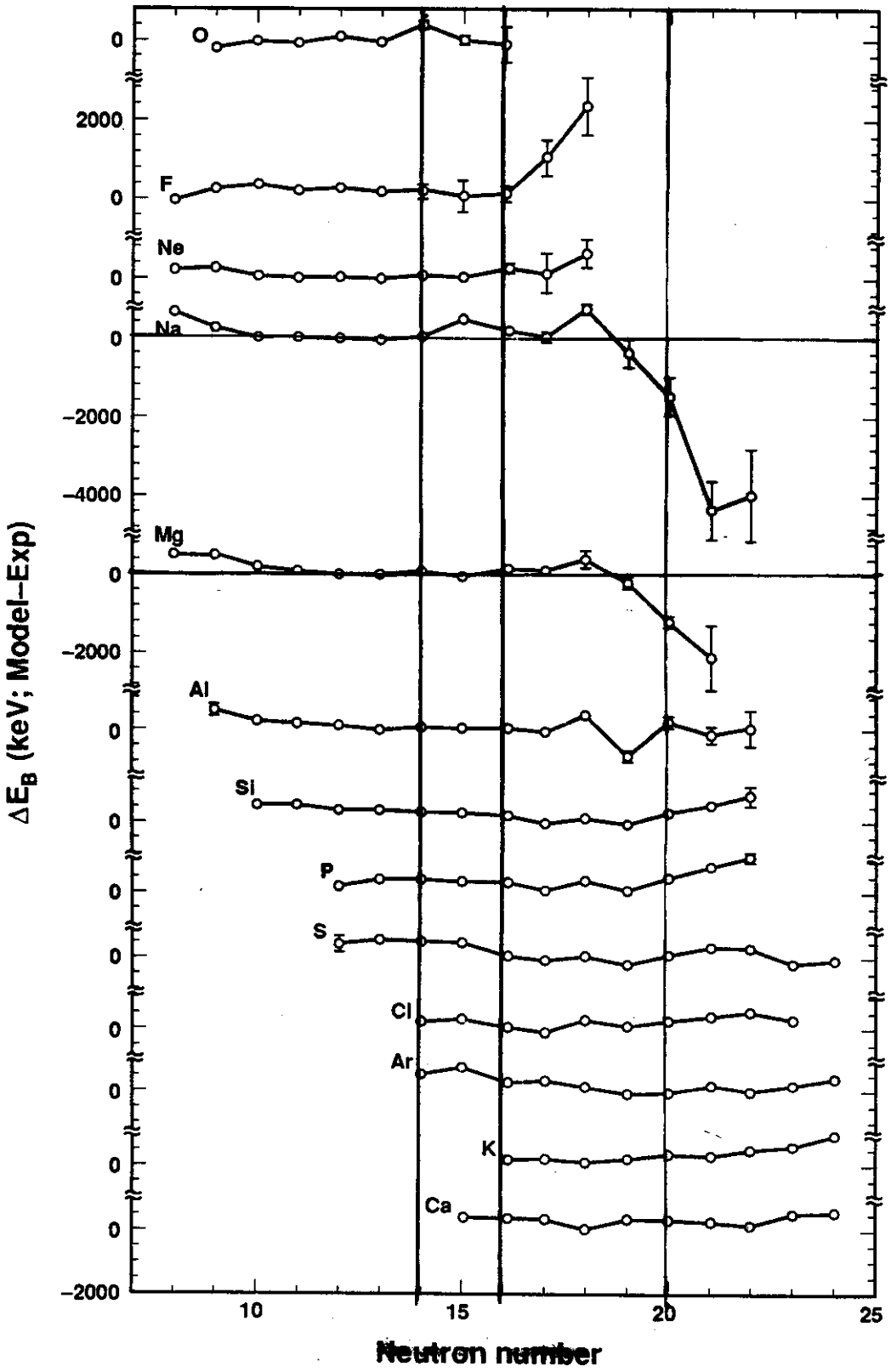
O
F
Ne
Na
Mg
Al
Si
P
S
Cl
Ar
K
Ca
0
2000
0
0
0
-2000
-4000
0
-2000
0
0
0
0
0
0
0
-2000
10
15
20
25
Neutron number
ΔE_B (keV; Model-Exp)

FIGURE 5

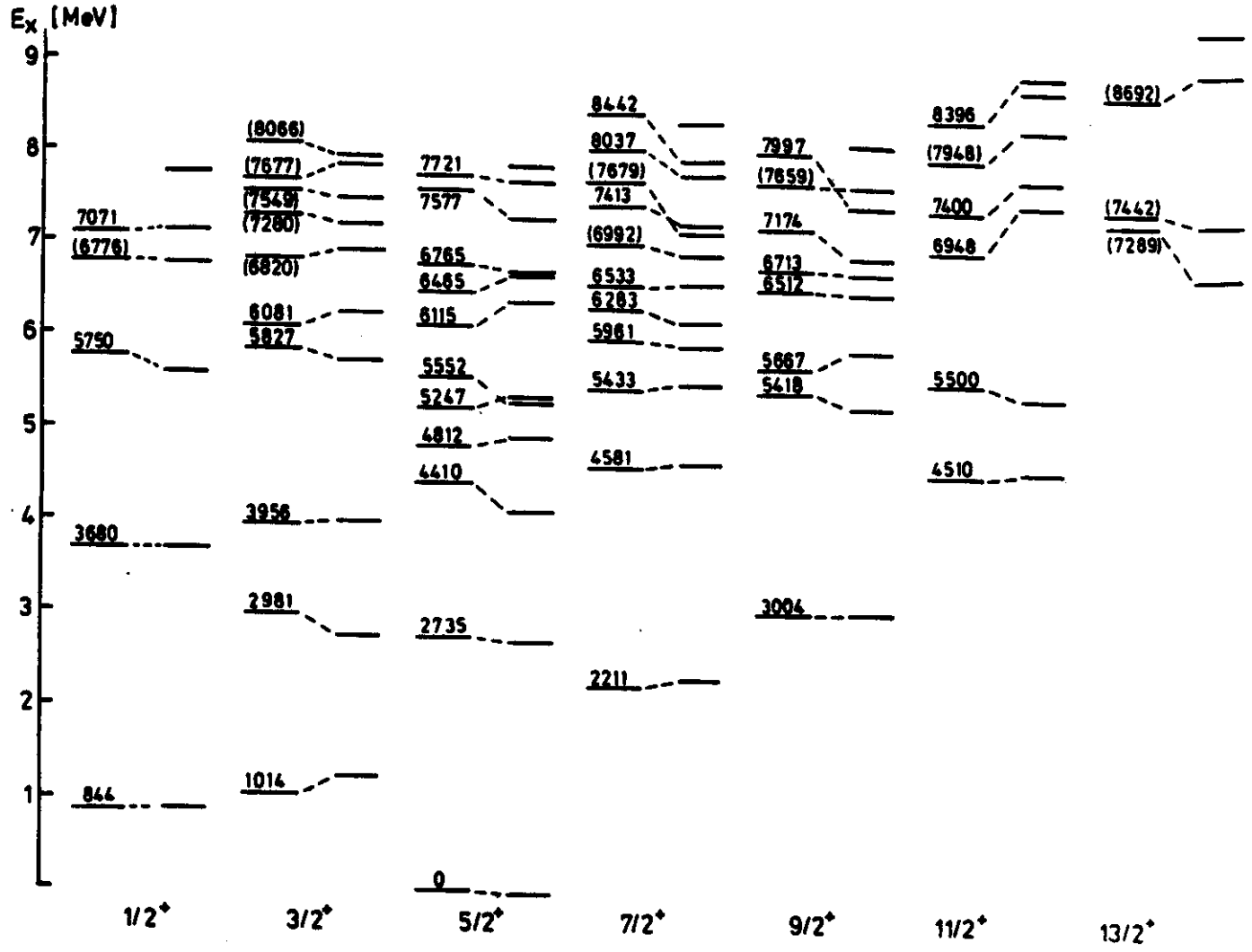
Ex [MeV]
9
8
7
6
5
4
3
2
1
7071
(6776)
5790
3680
844
(8066)
(7677)
(7549)
(7280)
(6820)
6081
5827
3956
2981
1014
7721
7577
6765
6485
6115
5552
5247
4812
4410
2735
0
8442
8037
(7679)
7413
(6992)
6533
6283
5961
5433
4581
2211
7997
(7659)
7174
6713
6512
5667
5418
3004
8396
(7948)
7400
6948
5500
4510
(8692)
(7442)
(7289)
1/2+
3/2+
5/2+
7/2+
9/2+
11/2+
13/2+

FIGURE 6

Z/N	18	19	20	21	22	23
15	^{33}P +4839:W	^{34}P +3781:W	^{35}P +2698:W	^{36}P +2811:W	^{37}P *D(1/2)* **18823*	^{38}P *D(4$^-$)* *149590*
14	^{32}Si +4134:W	^{33}Si +2716:W	^{34}Si +1816:W +1554:T	^{35}Si +2063:W	^{36}Si +2261:W	^{37}Si *D(7/2)* *169606*
13	^{31}Al +3396:W	^{32}Al +2214:W	^{33}Al +854:W	^{34}Al +786:W	^{35}Al *D(5/2)* **46116*	^{36}Al *D(4$^-$)* *149590*
12	^{30}Mg +2104:W	^{31}Mg +780:W	^{32}Mg − 926:W −966:T	^{33}Mg −1090:W	^{34}Mg − 685:W	^{35}Mg *D(3/2)* **62787*
11	^{29}Na +2317:W	^{30}Na +776:W	^{31}Na −502:W −764:T	^{32}Na −1295:W	^{33}Na − 427:W	^{34}Na *D(4$^-$)** **44735*
10	^{28}Ne +1843:W	^{29}Ne +609:W	^{30}Ne − 698:W − 788:F	^{31}Ne − 891:W	^{32}Ne − 128:W	^{33}Ne + 480:W
9	^{27}F +3273:W	^{28}F +2110:W +2251:F	^{29}F +1286:W +1338:F	^{30}F +1444:W	^{31}F +1329:W	^{32}F +1557:W
8	^{26}O +4246:W +4495:F	^{27}O +3550:W +3568:F	^{28}O +3038:W +2956:F	^{29}O +2870:W +2904:F	^{30}O +2945:W +2905:F	^{31}O +2768:W

FIGURE 7

Z/N	18	19	20	21	22	23
15	^{33}P +5720:W *****:F *****:3	^{34}P +1673:W *****:F *****:3	^{35}P +4637:W +4290:F +8531:3	^{36}P +1025:W *****:F *****:3	^{37}P +4750:W *****:F *****:3	^{38}P *****:W *****:F *****:3
14	^{32}Si +5647:W *****:F *****:3	^{33}Si + 935:W *****:F *****:3	^{34}Si +4747:W +4227:F +7710:3	^{35}Si + 881:W *****:F +4042:3	^{36}Si +4994:W *****:F *****:3	^{37}Si +1079:W *****:F *****:3
13	^{31}Al +4505:W *****:F *****:3	^{32}Al + 959:W *****:F *****:3	^{33}Al +3145:W +3086:F +5291:3	^{34}Al − 105:W *****:F *****:3	^{35}Al +3077:W *****:F *****:3	^{36}Al *****:W *****:F *****:3
12	^{30}Mg +4678:W *****:F +8024:3	^{31}Mg + 8:W *****:F +1948:3	^{32}Mg +2972:W +2484:F +3588:3	^{33}Mg − 934:W − 729:F + 87:3	^{34}Mg +2808:W *****:F *****:3	^{35}Mg − 529:W *****:F *****;3
11	^{29}Na +3682:W *****:F +6142:3	^{30}Na + 306:W − 87:F +1830:3	^{31}Na +2404:W +2083:F +2387:3	^{32}Na − 808:W −1347:F + 43:3	^{33}Na +1611:W *****:F *****:3	^{34}Na + 60:W *****:F *****:3
10	^{28}Ne +4426:W +3939:F +7108:3	^{29}Ne + 211:W + 123:F +1861:3	^{30}Ne +3119:W +2666:F +3535:3	^{31}Ne − 909:W −1192:F + 270:3	^{32}Ne +2926:W *****:F +4713:3	^{33}Ne − 146:W *****:F +2371:3
9	^{27}F +3538:W +3821:F +8567:3	^{28}F + 662:W + 687:F +4093:3	^{29}F +2714:W +2721:F +4982:3	^{30}F + 624:W + 630:F +2777:3	^{31}F +2872:W +2780:F +5253:3	^{32}F + 509:W *****:F +2887:3
8	^{26}O + 5480:W + 4808:F +11488:3	^{27}O +2110:W +2015:F +6188:3	^{28}O +4972:W +4255:F +8354:3	^{29}O + 928:W + 833:F +4383:3	^{30}O +4804:W +4020:F +8084:3	^{31}O +1003:W + 878:F +4408:3

FIGURE 8

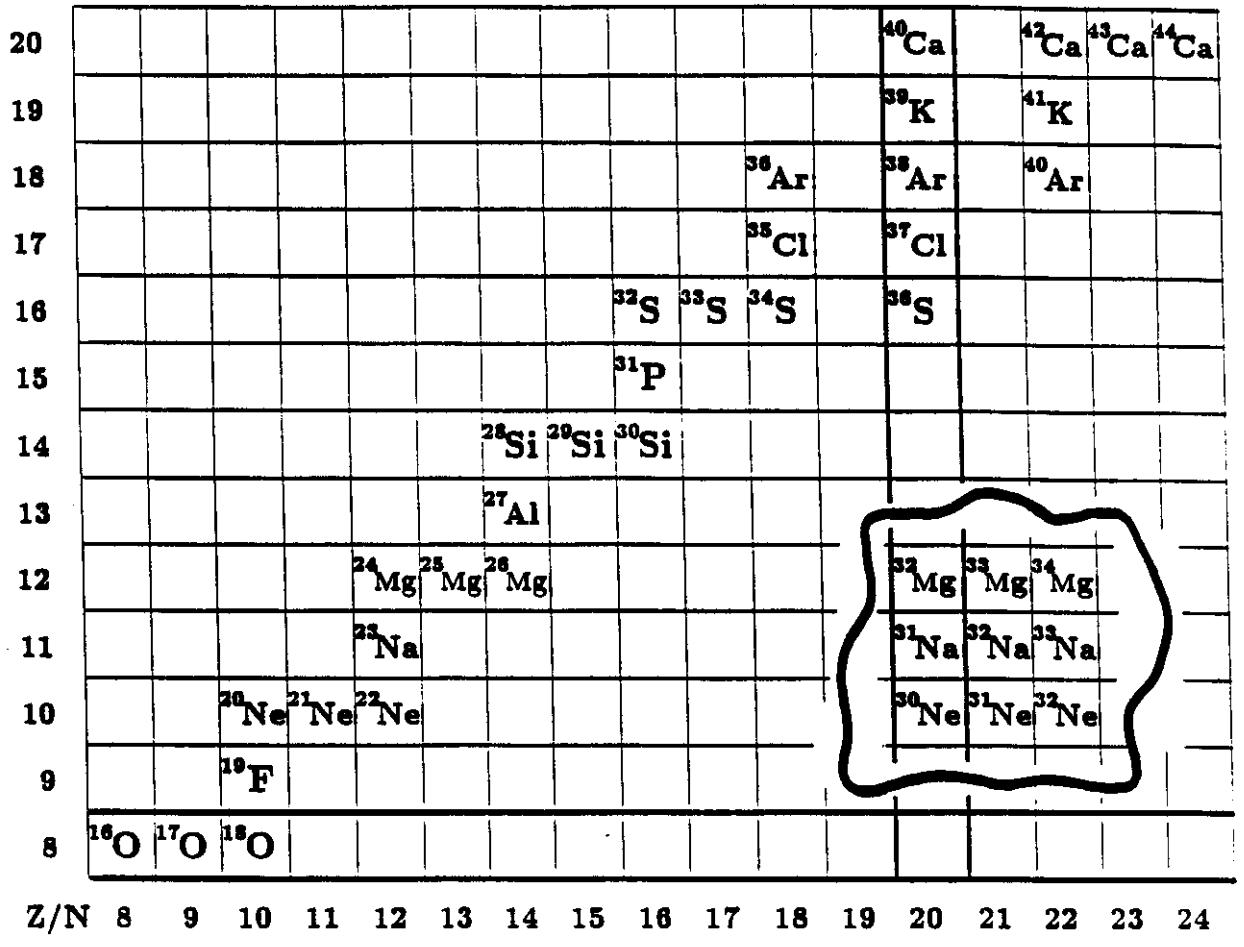
20
19
18
17
16
15
14
13
12
11
10
9
8
Z/N 8 9 10 11 12 13 14 15 16 17 18 19 20 21 22 23 24
^{16}O ^{17}O ^{18}O
^{19}F
^{20}Ne ^{21}Ne ^{22}Ne
^{23}Na
^{24}Mg ^{25}Mg ^{26}Mg
^{27}Al
^{28}Si ^{29}Si ^{30}Si
^{31}P
^{32}S ^{33}S ^{34}S
^{35}Cl
^{36}Ar
^{37}Cl
^{38}Ar
^{39}K
^{40}Ca
^{41}K
^{42}Ca ^{43}Ca ^{44}Ca
^{30}Ne ^{31}Ne ^{32}Ne
^{31}Na ^{32}Na ^{33}Na
^{32}Mg ^{33}Mg ^{34}Mg
^{40}Ar

FIGURE 9

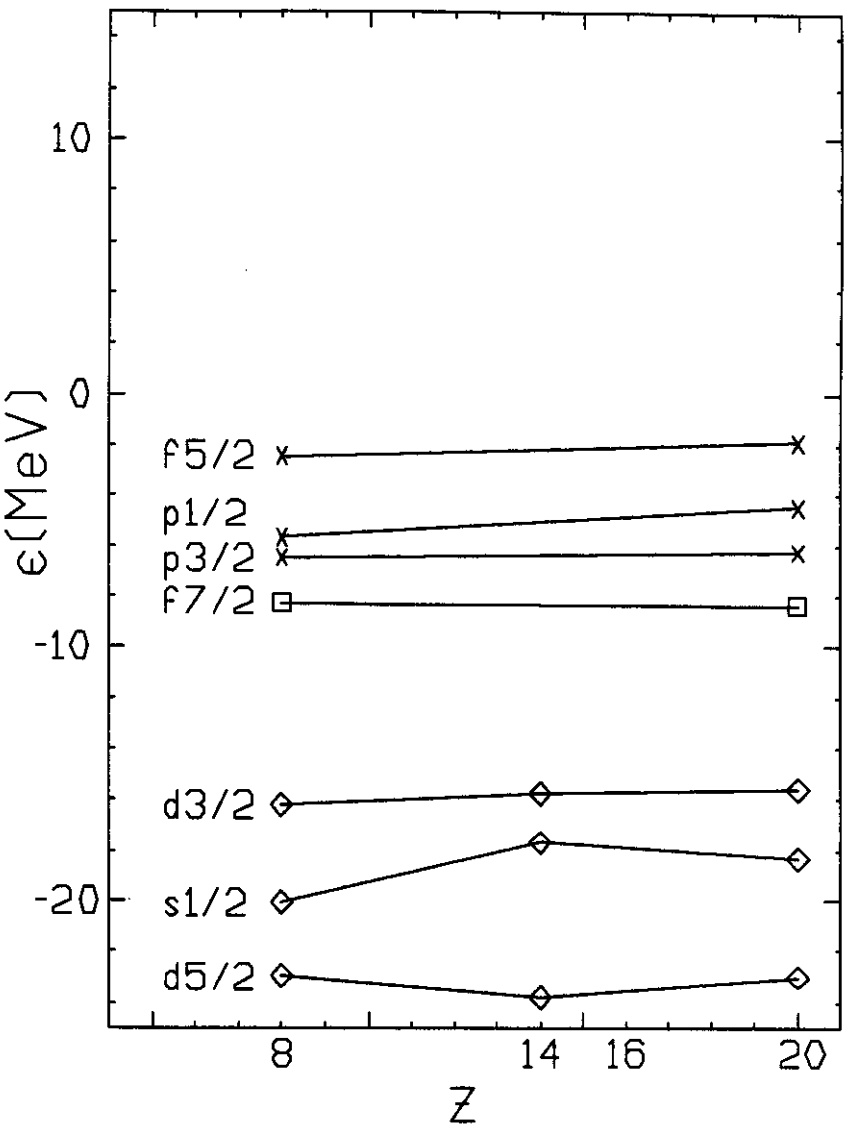

FIGURE 10

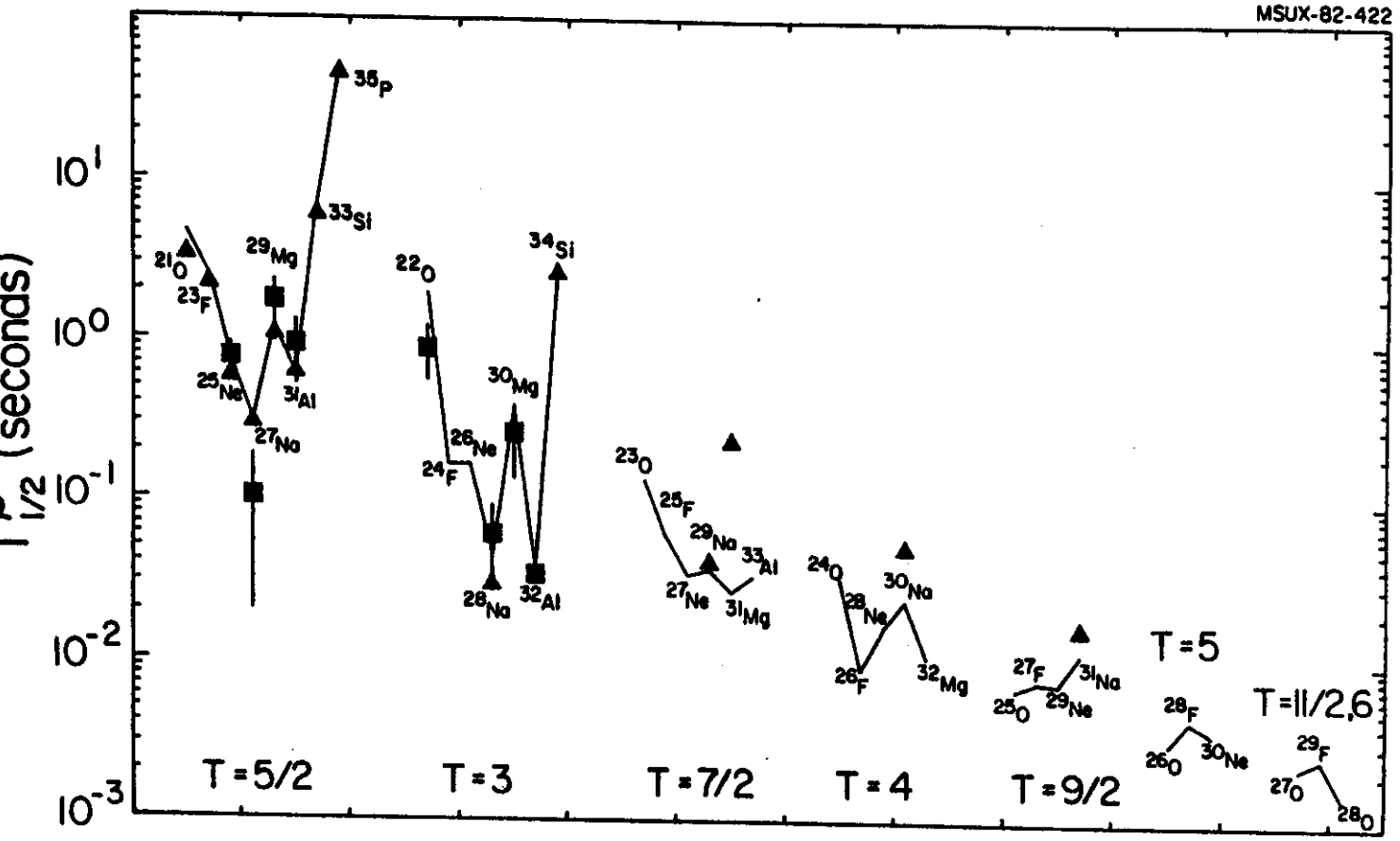
MSUX-82-422
$T_{1/2}$ (seconds)
10^{1}
10^{0}
10^{-1}
10^{-2}
10^{-3}
^{21}O
^{23}F
^{25}Ne
^{27}Na
^{29}Mg
^{31}Al
^{33}Si
^{35}P
^{22}O
^{24}F
^{26}Ne
^{28}Na
^{30}Mg
^{32}Al
^{34}Si
^{23}O
^{25}F
^{27}Ne
^{29}Na
^{31}Mg
^{33}Al
^{24}O
^{26}F
^{28}Ne
^{30}Na
^{32}Mg
^{25}O
^{27}F
^{29}Ne
^{31}Na
^{26}O
^{28}F
^{30}Ne
^{27}O
^{29}F
^{28}O
T = 5/2
T = 3
T = 7/2
T = 4
T = 9/2
T = 5
T = 11/2, 6

FIGURE 11

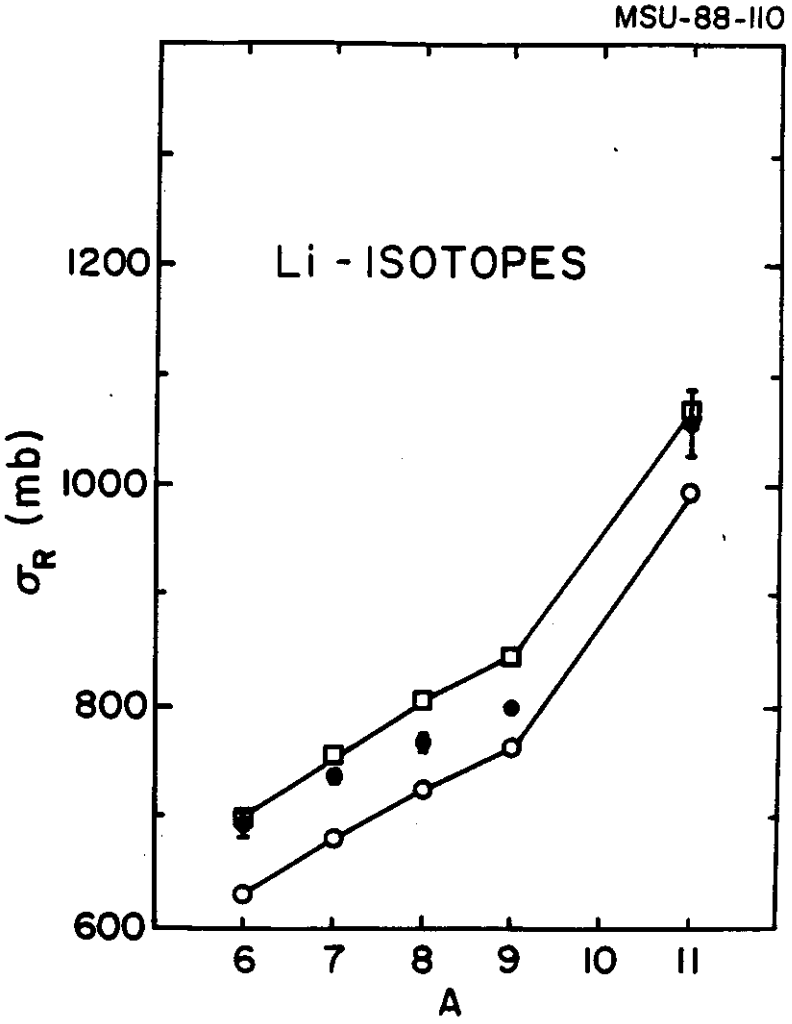

FIGURE 12a

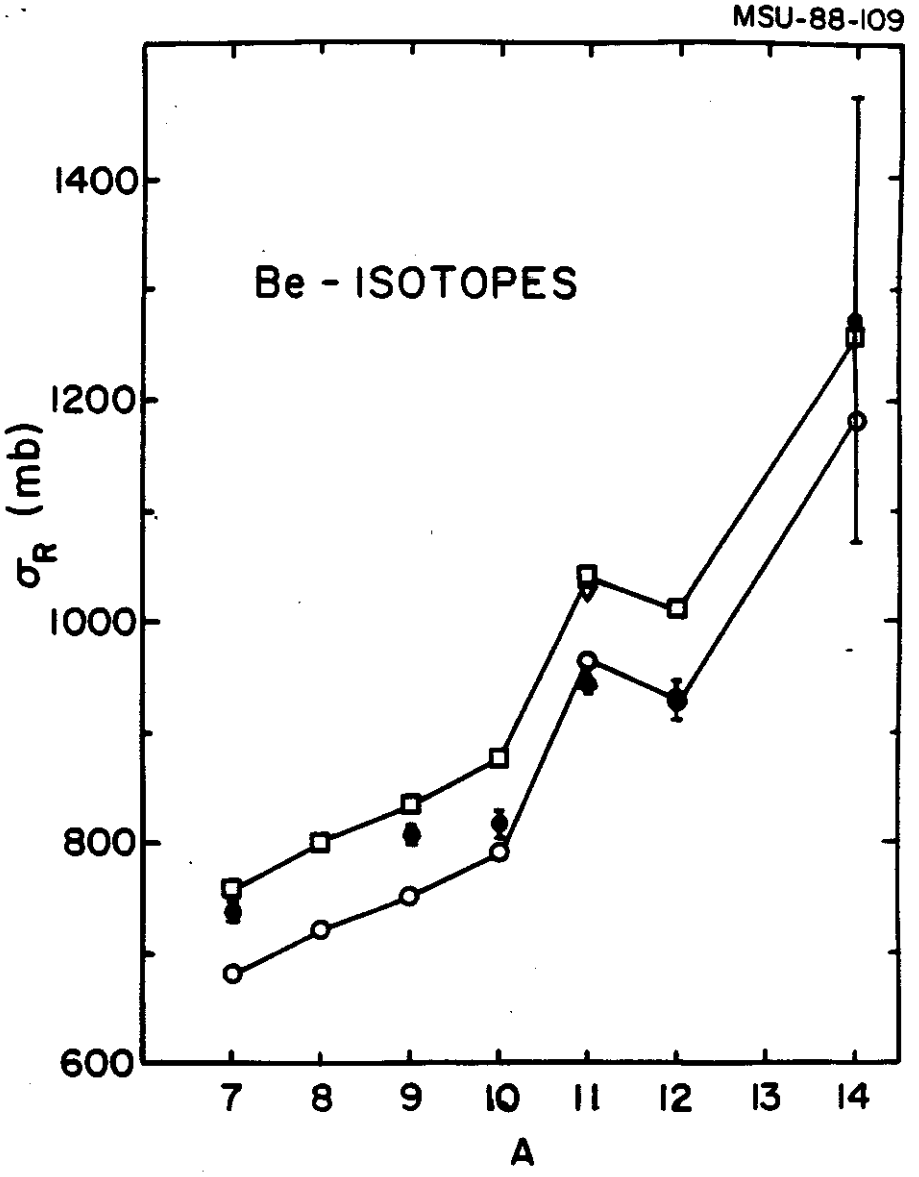

FIGURE 12b